

## Organization of the Olfactory and Respiratory Skeleton in the Nose of the Gray Short-Tailed Opossum *Monodelphis domestica*

Timothy B. Rowe,<sup>1,2,3</sup> Thomas P. Eiting,<sup>1</sup> Thomas E. Macrini,<sup>1</sup>  
and Richard A. Ketcham<sup>1</sup>

---

The internal nasal skeleton in *Monodelphis domestica*, the gray short-tailed opossum, primarily supports olfactory and respiratory epithelia, the vomeronasal organ, and the nasal gland. This scaffold is built by the median mesethmoid, and the paired vomer and ethmoid bones. The mesethmoid ossifies within the nasal septum cartilage. The bilateral ethmoid segregates respiratory and olfactory regions, and its geometry offers insight into the functional, developmental, and genomic organization of the nose. It forms through partial coalescence of separate elements known as turbinals, which in *Monodelphis* comprise the maxilloturbinal, nasoturbinal, five endoturbinals, and two ectoturbinals. Geometry of the ethmoid increases respiratory mucosal surface area by a factor of six and olfactory mucosal surface by nearly an order of magnitude. Respiratory epithelium warms and humidifies inspired air, recovers moisture as air is exhaled, and may help mediate brain temperature. In contrast, the olfactory skeleton functions as a series of small funnels that support growth of new olfactory neurons throughout life. Olfactory mucosa lines the mouth of each funnel, forming blind olfactory recesses known as the ethmoid cells, and neuronal axons are funneled from the epithelium through tiny olfactory foramina in the cribriform plate, into close proximity with target glomeruli in the olfactory bulb of the brain where each axon makes its first synapse. The skeleton may thus mediate topological correspondence between odorant receptor areas in the nose with particular glomeruli in the olfactory bulb, enabling growth throughout life of new olfactory neurons and proper targeting by their axons. The geometric arrangement of odorant receptors suggests that a measure of volatility may be a component in the peripheral olfactory code, and that corresponding glomeruli may function in temporal signal processing. Supporting visualizations for this study are available online at [www.DigiMorph.org](http://www.DigiMorph.org).

---

**KEY WORDS:** Vomeronasal organ, Mesethmoid, Ethmoid, Turbinals, Vomer, Computed tomography.

### INTRODUCTION

Mammals live in an olfactory world to a greater degree than perhaps any other air-breathing creature. Olfaction mediates food detection, species isolation, social integration, myriad reproductive processes, alarm and defense, orientation and navigation, and a host of other

---

<sup>1</sup>Jackson School of Geosciences, The University of Texas at Austin, Austin, Texas 78712, USA.

<sup>2</sup>Texas Memorial Museum, The University of Texas at Austin, Austin, Texas 78712, USA.

<sup>3</sup>To whom correspondence should be addressed at The University of Texas at Austin, Geol. Science Department, 1 University Station C1100, Austin, Texas 78712-0254, USA. E-mail: [rowe@mail.utexas.edu](mailto:rowe@mail.utexas.edu)

functions (Stoddart, 1980a,b). The mammalian nose also functions in respiratory physiology, by regulating water balance and heat exchange in a role believed critical in mammalian endothermy (Schmidt-Nielsen *et al.*, 1970; Van Valkenburgh *et al.*, 2004).

Both olfaction and respiration are initiated in epithelia that line the nose and are spread over an elaborate internal skeleton. Renewed interest in this region was spawned by discovery that an order of magnitude more genes code for olfactory odorant receptors (ORs) in the mouse (*Mus musculus*) than in any other chordate yet sampled. G-protein-coupled ORs in the nose are encoded by nearly 1000 genes. They comprise between 1 and 5% of the total mouse genome and form its largest single gene family (Buck and Axel, 1991; Ressler *et al.*, 1993, 1994). Comparative analyses indicate that the number of OR genes is variable among mammals (Rouquier *et al.*, 2000). The mouse has 913 intact OR genes and 256 OR pseudogenes (Godfrey *et al.*, 2004), while humans have 339 intact OR genes and 297 pseudogenes (Malnic *et al.*, 2004). Some OR gene subfamilies are conserved between species, but each species has subfamilies that are not present in the other, suggesting that the olfactory genome has undergone a complex evolutionary history in mammals (Lane *et al.*, 2001). Elaborate diversification of the internal skeleton of the nose may correspondingly reflect the evolution of genomic complexity.

The respiratory and olfactory epithelia are arrayed over paper-thin filigreed scrolls, arbors, and plates of bone known collectively as turbinals (Owen, 1854). While the turbinals may seem hopelessly fragile, they support erectile tissues and glands (Salazar *et al.*, 1997), and much of their surface area lies within the air currents of respiration (Proetz, 1953; Negus, 1958), suggesting that complex mechanical loads are borne by this scaffold.

Turbinals develop from the membranous lining of the embryonic olfactory capsule to anchor an expansive epithelium in a way that provides for its growth over many weeks of postnatal development. This skeleton provides a rigid armature that maintains geometrically complex air-filled spaces and passageways, through which air passes and odorant molecules disperse in the course of normal functioning of the nose. It also provides for compartmentalization of olfactory and respiratory regions within the nose. Mammals are unique in the extent to which this internal skeleton is elaborated (Gauthier *et al.*, 1988; Rowe, 1988, 1993).

These bones and their attendant passageways are the least-studied region of the skeleton, yet they comprise nearly half the volume of the skull in small species. The external anatomy of the nose is well known in most mammals, including didelphids (Coues, 1872; Clark and Smith, 1993; Marshall and de Muizon, 1995; Wible, 2003), but the internal skeleton is only vaguely known for most living species and is virtually *terra incognita* in fossil mammals. Variability in this complex is suspected to be systematically informative (Cleland, 1862; Allen, 1882; Paulli, 1900a,b,c; Gregory, 1910; Negus, 1958; Moore, 1981; Novacek, 1993). However, few characters are formally scored in cladistic analyses, variability of this system is not well represented in phylogenetic data matrices (but see Gauthier *et al.*, 1988; Rowe, 1988, 1993; Voss and Jansa, 2003), and our understanding of how the nose “works” and evolved in mammals remains incomplete.

Difficulties in studying the internal skeleton of the nose derive from its delicate intricacy and remoteness from direct observation. High-resolution X-ray computed tomography (HRXCT; Rowe *et al.*, 1993, 1995, 1997, 1999; Carlson *et al.*, 2003) is now making possible measurement and comparison of the surfaces, partial volumes, and passageways of the nose (Van Valkenburgh *et al.*, 2004). We employed HRXCT along with conventional histological sectioning as the basis for a quantitative description of the internal skeleton of

the nose in *Monodelphis domestica*. We also draw on functional and neurological studies of the nose in other mammals, insofar as neural projections and function of this system appear highly conserved among mammals and indeed among tetrapods generally (e.g., Butler and Hodos, 1996; Nieuwenhuys *et al.*, 1998).

Another problem in the nose is the nomenclature of its parts. Over the last 200 years singular terms have been applied by various authors to different structures, and several have expressed frustration with the situation (e.g., Cleland, 1862; Allen, 1882; Moore, 1981; see also Witmer, 1995). We make no attempt to untangle historic conflicts in usage or priority, but rather we try to be explicit in the meanings of the anatomical terms as they are employed below. Probably our only unprecedented construct is in grouping the maxilloturbinal and nasoturbinal as parts of the more inclusive ethmoid bone, rather than as separate elements in the nose. Because these elements all arise in the epithelium of the nasal capsule, their developmental hierarchy can be reflected profitably in a hierarchical anatomical nomenclature (Rowe, 1986) that categorizes the nasoturbinal and maxilloturbinal as parts of the more inclusive ethmoid bone.

The new ability to map its internal skeletal anatomy may offer a new light in which to view other levels of organization in the mammalian nose. For example, at the cellular level, a recalcitrant problem surrounds the mechanism of axonal guidance over the full course of neuronal ontogeny. OR neurons are short-lived and new cells are generated throughout ontogeny from stem cells in the olfactory epithelium. The axons of these new nerves find their way to the proper receptors in the olfactory bulb, making their first synapse in tiny neural targets known as glomeruli. Experimental data indicate that olfactory axons have no extrinsic guidance mechanism until they reach the brain itself and only upon encountering cerebral tissue does a guidance mechanism affect their course, leading them to their proper glomerulus (Berlingrood, 1969). How the new axons traverse broad distances from ORs in the epithelium to such exacting targets remains unexplained (Mombaerts, 1999; Dryer, 2000).

At the molecular level, there is uncertainty about the fundamental nature of the peripheral olfactory code (Dreyer, 1998; Laurent, 1999; Rubin and Katz, 1999). The olfactory system has an open design, like the immune system, built on the premise that it is not possible to predict *a priori* what molecules might enter the nose (Firestein, 2001). Peripheral coding is hypothesized to be based on activation of arrays of OR cells with overlapping tuning profiles (Ducham-Viret *et al.*, 1999). ORs are organized into a series of expression zones, in which multiple copies of a small number of receptor types are distributed. Neurons expressing the same receptor subfamilies are not clustered, but rather are distributed stochastically about the zone. Odor intensity is based on the number of cells activated. However, it is less clear how identity of a virtually infinite array of molecules is encoded. Even with 1000 different odorant receptors, the number of odors that mammals can recognize is exponentially greater, and thus the exact nature of the peripheral olfactory code is unclear. A combinatorial model may explain subsequent higher levels of processing, but this must occur in post-glomerular processing rather than at the level of the olfactory membrane itself (Mori *et al.*, 1999). What exactly is being encoded at the olfactory membrane, transmitted, and decoded in the first synapse in the olfactory bulb?

In detailing the internal morphology of the nose in *Monodelphis*, we argue that insight into each of these questions may lie in the more general organization of the internal skeleton of the nose.

## MATERIALS AND METHODS

This study is based on a growth series of *Monodelphis domestica* specimens of precisely documented ages commissioned from the Southwest Foundation for Biomedical Research in San Antonio, TX (e.g., VandeBerg, 1990) for the Vertebrate Paleontology Laboratory of the Texas Memorial Museum (TMM). The collection includes serial-sectioned histological preparations (azocarmine) of five specimens (aged day 0, 10, 15, 26, and 36 postnatal), over 120 cleared and double-stained whole preparations (aged from day 0 through retired breeders), and 30 dried skeletons representing different ages. The histological serial sections were studied to trace development of the turbinals, epithelial differentiation, nerve pathways, and they also provided landmarks for interpreting the distributions of different epithelial types in HRXCT scans. Fifteen specimens were CT scanned at the University of Texas High-Resolution X-ray Computed Tomography Facility (Rowe *et al.*, 1997). The scanned specimens ranged from 27-day-old specimens through retired breeders, and included dried, ETOH preserved, and frozen whole individuals. A description of the HRXCT equipment used, as well as an introduction to HRXCT principles and their application to natural specimens, is provided by Ketcham and Carlson (2001).

The CT dataset plus derivative digital visualizations are available on the Internet (Table I) and in Macrini (2000). Throughout the text, references are made to sequentially numbered CT images of the skull of TMM M-7599. The image plane (i.e., coronal, horizontal, or sagittal; see Fig. 1) is given as a prefix followed by the specific image number. For example, C100 refers to coronal image number 100. Consecutive image sequences are rendered with a dash. Different parts of the ethmoid are color-coded on some of the CT images. In the text below, the color for a particular structure is indicated in parentheses in the appropriate section describing that structure.

A quantitative analysis of a single adult specimen (TMM M-7599; Figs. 1–4) is summarized in Table II. Measurements of surface areas and partial volumes for the right nasal chamber and its skeleton were taken using Blob3D software (Ketcham, 2005). We also measured surface areas and volumes of individual bony elements, as well as surface areas and volumes of olfactory and respiratory regions, which are spread over several skeletal elements. All measurements are based on the bony skeleton rather than the epithelia themselves, but we assumed that the difference in the two measures is negligible for the general purposes of our discussion below. Because the basic nature of the internal skeleton of the nose is to provide for expansion in surface area of its overlying epithelium, we measured turbinal volumes and calculated the surface area of spheres of equivalent volumes as a basis for comparison of both surface area and shape. For example, the ratio of observed surface area to sphere-equivalent surface area ranged from 3.25 (ectoturbinal II) to 6.00 (maxilloturbinal). By this measure, the maxilloturbinal departs further from a sphere than any other element.

## RESULTS

### Internal Skeleton of the Nose

The external skeleton of the nose in adult *Monodelphis* forms a rigid shell that anchors the internal skeleton and encloses an elaborate internal space. The external skeleton consists of the paired premaxilla, maxilla, nasal, lacrimal, frontal, palatine and orbitosphenoid bones (Figs. 2–4). The first of these bones form the snout and roof of the mouth, while the last

**Table I.** List of *Monodelphis Domestica* Movies on www.digimorph.org

| Specimen   | Age <sup>a</sup> | Movie  | URL  |
|------------|------------------|--|--|
| TMM M-7599 | Adult ♂          | Coronal slice <sup>b</sup><br>Horizontal slice<br>Sagittal slice<br>Roll spin 3-D <sup>c</sup><br>Pitch spin 3-D<br>Yaw spin 3-D<br>Roll spin endo <sup>d</sup><br>Roll spin both <sup>e</sup><br>Coronal slice colored turbinals <sup>f</sup>   | <a href="http://digimorph.org/specimens/Monodelphis_domestica/adult/index.phtml">http://digimorph.org/specimens/<br/>Monodelphis_domestica/adult/index.phtml</a>   |
| TMM M-7595 | Day 27           | Coronal slice<br>Horizontal slice<br>Sagittal slice<br>Roll spin 3-D<br>Pitch spin 3-D<br>Yaw spin 3-D   | <a href="http://digimorph.org/specimens/Monodelphis_domestica/day27/index.phtml">http://digimorph.org/specimens/<br/>Monodelphis_domestica/day27/index.phtml</a>   |
| TMM M-7536 | Day 48           | Coronal slice<br>Horizontal slice<br>Sagittal slice<br>Roll spin 3-D<br>Pitch spin 3-D<br>Yaw spin 3-D   | <a href="http://digimorph.org/specimens/Monodelphis_domestica/day48/index.phtml">http://digimorph.org/specimens/<br/>Monodelphis_domestica/day48/index.phtml</a>   |
| TMM M-7539 | Day 57           | Coronal slice<br>Horizontal slice<br>Sagittal slice<br>Roll spin 3-D<br>Pitch spin 3-D<br>Yaw spin 3-D   | <a href="http://digimorph.org/specimens/Monodelphis_domestica/day57/index.phtml">http://digimorph.org/specimens/<br/>Monodelphis_domestica/day57/index.phtml</a>   |
| TMM M-7542 | Day 75           | Coronal slice<br>Horizontal slice<br>Sagittal slice<br>Roll spin 3-D<br>Pitch spin 3-D<br>Yaw spin 3-D   | <a href="http://digimorph.org/specimens/Monodelphis_domestica/day75/index.phtml">http://digimorph.org/specimens/<br/>Monodelphis_domestica/day75/index.phtml</a>   |
| TMM M-7545 | Day 90           | Coronal slice<br>Horizontal slice<br>Sagittal slice<br>Roll spin 3-D<br>Pitch spin 3-D<br>Yaw spin 3-D   | <a href="http://digimorph.org/specimens/Monodelphis_domestica/day90/index.phtml">http://digimorph.org/specimens/<br/>Monodelphis_domestica/day90/index.phtml</a>   |
| TMM M-8273 | Adult ♂          | Coronal slice<br>Horizontal slice<br>Sagittal slice<br>Roll spin 3-D (skeleton only)<br>Pitch spin 3-D (skeleton only)<br>Yaw spin 3-D (skeleton only)<br>Roll spin 3-D (body with skin)<br>Pitch spin 3-D (body with skin)<br>Yaw spin 3-D (body with skin)<br>Roll spin 3-D (skull only)<br>Pitch spin 3-D (skull only)<br>Yaw spin 3-D (skull only)<br>Roll spin 3-D (head with skin)<br>Pitch spin 3-D (head with skin)<br>Yaw spin 3-D (head with skin) | <a href="http://digimorph.org/specimens/Monodelphis_domestica/whole/">http://digimorph.org/specimens/<br/>Monodelphis_domestica/whole/</a><br><br><a href="http://digimorph.org/specimens/Monodelphis_domestica/head/">http://digimorph.org/specimens/<br/>Monodelphis_domestica/head/</a> |

<sup>a</sup>Exact age is given in days postnatal, if known.

<sup>b</sup>Slice movies show CT images in one of three designated orthogonal planes (coronal, horizontal, or sagittal).

<sup>c</sup>3-D movies show volumetric renderings of either the skull, head, skeleton, or whole body rotating in either the roll, pitch, or yaw motion.

<sup>d</sup>“Roll spin endo” shows an isosurface model of the isolated cranial endocast rotating in roll spin motion.

<sup>e</sup>“Roll spin both” shows an isosurface model of the cranial endocast in its semi-transparent skull rotating in roll spin motion.

<sup>f</sup>“Coronal slice colored turbinals” is a coronal slice movie with the turbinals color coded. Key to colors is given in text and Figs. 5 and 13.

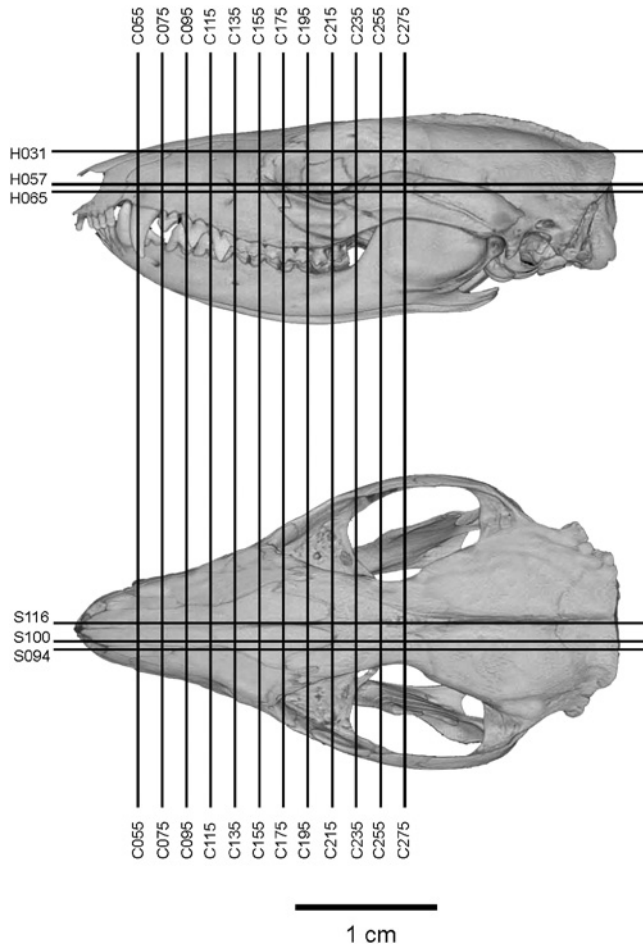


**Fig. 1.** Left lateral and dorsal views of the skull of TMM M-7599, showing the approximate locations of CT images in three orthogonal planes (C: coronal, H: horizontal, S: sagittal) that are depicted in Figs. 5–7 and 13. This imagery of the skull is a computer-generated 3D volumetric from the original HRXCT data (Table I).

form the rostral and medial walls of the orbit, lying deep to the eyeball and orbital glands. The ethmoid may also play a small role in the medial orbital wall. Collectively, these bones enclose the nasal cavity, whose total (bilateral) volume is approximately  $300 \text{ mm}^3$  (Table II). The nasal cavity is itself divided into the nasopharyngeal passageway, which comprises approximately 45% of the nasal cavity volume, and the sphenethmoid or olfactory recess, which comprises approximately 55% of the volume (Table II). As described below, these spaces are largely separated by an internal skeleton built from the median (unpaired) mesethmoid, the paired vomer, and the paired ethmoid (Table III, Figs. 5–8).

#### *Median Elements*

*Mesethmoid and Nasal Septum.* In all mammals studied, the nasal septum arises early in ontogeny from a median plate of neural crest cells lying between the paired olfactory

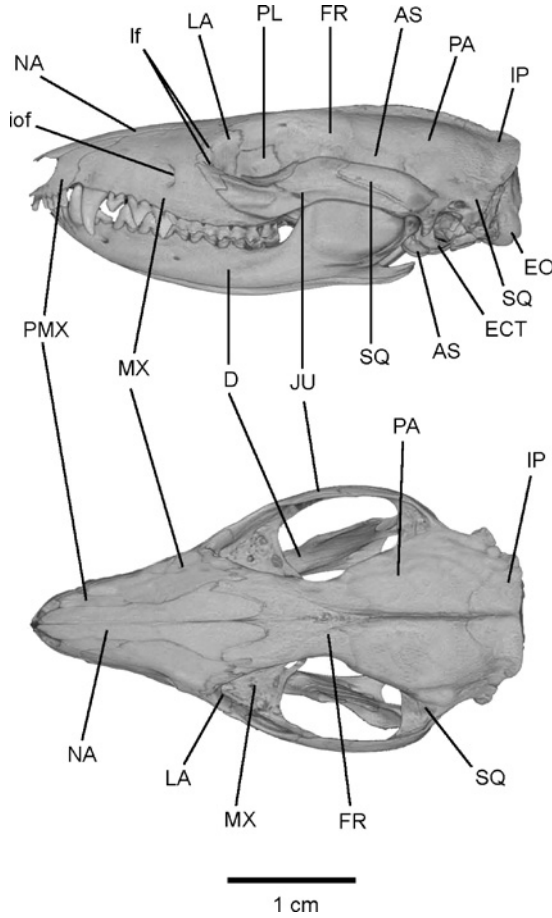


**Fig. 2.** Left lateral and dorsal views of the skull of TMM M-7599, an adult female *Monodelphis domestica*. This computer-generated 3D volumetric reconstruction of the skull was generated from the original HRXCT data (Table I). See Appendix I for key to abbreviations.

placodes (de Beer, 1937; Moore, 1981; Noden, 1990; Hall, 1990). The olfactory placodes originate in the ectoderm and “sink” from their superficial origin deep into the nose toward the developing forebrain, leaving the primordial nasal cavities in their wake. The right and left nasal cavities are separated by the median plate of neural crest cells that chondrifies to form the nasal septum (Fig. 5).

In *Monodelphis*, the nasal cavities and cartilaginous septum are present at birth. Subsequent ossification in the caudal part of the nasal septum produces the mesethmoid (Figs. 5–8). Ossification begins during the third postnatal week, from a single endochondral center immediately beneath the olfactory bulbs, and spreads slowly forward through the nasal septum as the snout elongates during eruption of the dentition. Ossification ends just in front of the upper canine, while rostral to this the nasal septum remains cartilaginous throughout life, protruding above the rostral spine of the premaxilla to support the rhinarium.

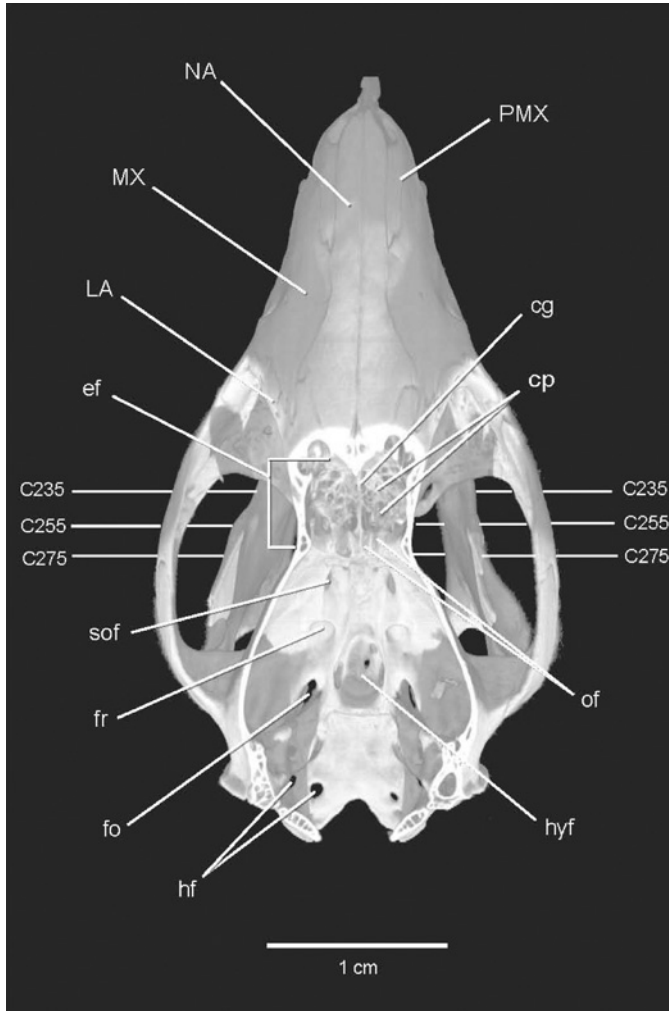


**Fig. 3.** Dorsal view of the skull of TMM M-7599, with the braincase roof digitally removed. The cut plane is at slight angle from horizontal. Horizontal lines key the locations of coronal HRXCT images in Fig. 5. See Appendix I for key to abbreviations.

At birth, the nasal septum in *Monodelphis* is a vertical plate over most of its length, but in the vicinity of the olfactory bulbs its superior edge projects laterally as a sheet of cartilage that forms the nasal tectum. In adults it may coossify with the frontal and nasal above the olfactory recess. The lateral edge of the nasal tectum provides the initial attachment base of the nasoturbinal (below). As ossification of this region proceeds, a complex of longitudinal ethmoid canals encloses fascicles of the terminal (CN 0) and vomeronasal nerves, and the rostral ethmoid branches of the ophthalmic artery and ophthalmic nerve (CN V<sub>1</sub>).

The mature mesethmoid participates in the rostral wall of the endocranial cavity where its superior edge forms the crista galli (Fig. 3), which protrudes for a short distance between

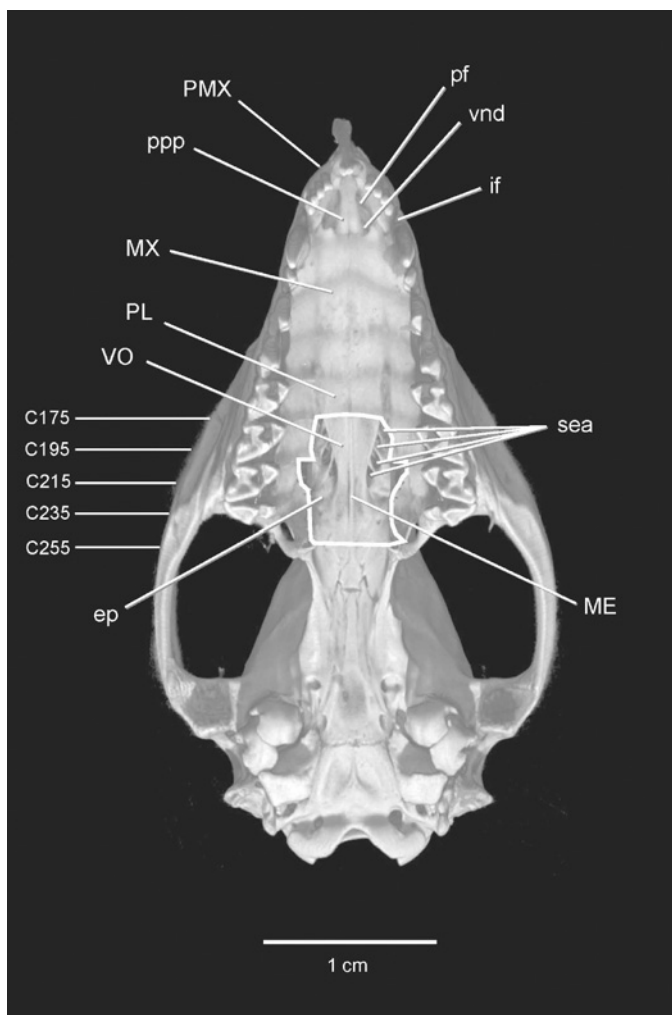


**Fig. 4.** Ventral view of the skull of TMM M-7599, with a portion of the palate removed (indicated by white outline). Horizontal lines indicate approximate locations of coronal CT images through this portion of the palate that are depicted in Fig. 5. This imagery of the skull is a computer-generated 3D volumetric from the original HRXCT data (Table I). See Appendix I for key to abbreviations.

the olfactory bulbs. To each side of the crista galli are attached the right and left cribriform plates of the ethmoid bone (below), which together enclose the endocranial ethmoid fossa and separate it from the nasal cavity (Fig. 3). In mature individuals, the cribriform plate and crista galli are completely co-ossified adjacent to the olfactory bulbs.

The inferior edge of the mesethmoid rests in a groove along the superior edge of the rostral process of the vomers, but does not fuse to the vomers at any stage in ontogeny that we observed. The tongue-in-groove relationship ceases at the confluence of the right and left nasopharyngeal meati, as they enter into the choana. There the inferior edge of the

**Table II.** Measurements of Individual Turbinals and Nasal Passageways<sup>a</sup>

| Component                | Volume<br>(mm <sup>3</sup> ) <sup>b</sup> | Surface area<br>(mm <sup>2</sup> ) <sup>c</sup> | Sph-equiv<br>radius <sup>d</sup> | Sph-equiv<br>SA <sup>e</sup> | SA/Sph<br>SA <sup>f</sup> | Beginning<br>slice | Ending<br>slice |
|--------------------------|---|---|----------------------------------|------------------------------|---------------------------|--------------------|-----------------|
| Nasal skeleton           |   |   |                                  |                              |                           |                    |                 |
| Respiratory turbinals    |   |   |                                  |                              |                           |                    |                 |
| Maxilloturbinal          | 15.869                                    | 183.097   | 1.559                            | 30.54                        | 6.00                      | 38                 | 196             |
| Endoturbinal I component | 3.754                                     | 47.227  | 0.964                            | 11.68                        | 4.04                      | 121                | 237             |
| Total                    | 19.623                                    | 230.324   | 1.673                            | 35.18                        | 6.55                      | 38                 | 237             |
| Olfactory turbinals      |   |   |                                  |                              |                           |                    |                 |
| Endoturbinal I component | 10.178                                    | 124.108   | 1.344                            | 22.71                        | 5.46                      | 121                | 237             |
| Endoturbinal II          | 2.092                                     | 27.149  | 0.793                            | 7.91                         | 3.43                      | 171                | 245             |
| Endoturbinal III         | 1.567                                     | 23.908  | 0.720                            | 6.52                         | 3.67                      | 197                | 250             |
| Endoturbinal IV          | 2.234                                     | 28.811  | 0.811                            | 8.26                         | 3.49                      | 192                | 265             |
| Endoturbinal V           | 3.447                                     | 48.946  | 0.937                            | 11.04                        | 4.44                      | 203                | 281             |
| Ectoturbinal I           | 3.482                                     | 43.333  | 0.940                            | 11.11                        | 3.90                      | 168                | 237             |
| Ectoturbinal II          | 2.654                                     | 38.609  | 0.859                            | 9.27                         | 4.16                      | 174                | 234             |
| Nasoturbinal component   | 2.465                                     | 28.672  | 0.838                            | 8.82                         | 3.25                      | 125                | 219             |
| Total                    | 28.119                                    | 363.536   | 1.886                            | 44.72                        | 8.13                      | 121                | 281             |
| Passageways              |   |   |                                  |                              |                           |                    |                 |
| Respiratory              | 72.240                                    | 368.620   | 2.584                            | 83.88                        | 4.39                      | 40                 | 248             |
| Olfactory                | 78.092                                    | 447.024   | 2.652                            | 88.35                        | 5.06                      | 119                | 281             |

<sup>a</sup>Measurements were taken from scans of a dried skull, hence the actual area of epithelium is somewhat greater than that reported for the bones themselves.

<sup>b</sup>Exact value of volume in cubic millimeters for each individual component listed.

<sup>c</sup>Surface area in square millimeters for each component listed.

<sup>d</sup>Represents the conversion of the volume data into a spherical volume followed by extracting the radius from this sphere-normalized value.

<sup>e</sup>Represents the surface area of the volume when that volume is considered to be a sphere. In this case, it is calculated from the sph-equiv radius.

<sup>f</sup>Ratio of the surface area generated by the data to the equivalent surface area of a spherical volume of the same size. In this case, it is calculated by dividing the surface area over the sph-equiv surface area. Values above 1 indicate an increase in surface area over what would be expected were the given component simply a sphere.

mesethmoid is exposed as a thin strip of bone along the midline of the roof of the choana, where it is clasped by the choanal process of the right and left vomers. The mesethmoid ends caudally inside the nose, at the back of the sphenethmoid recess, where it joins the orbitosphenoid at a point near the optic chiasm.

Histological sections indicate that the nasal surface of the mesethmoid is covered by typical olfactory epithelium. However, this epithelium is innervated by dendrites of the terminal nerve, and hence may play a different role in odorant perception (below) than epithelium arrayed over the ethmoid turbinals, which carries dendrites of the olfactory nerve (CN I).

The mesethmoid is sometimes viewed as a component of the "ethmoid bone" because these elements coossify in adults. However, in embryology, function, and phylogeny the mesethmoid and ethmoid are distinct (Table III). Whereas the mesethmoid ossifies from a single, median endochondral center, the ethmoid grows via the coalescence of multiple bilateral perichondral ossifications which arise in the membranous lining of the olfactory capsule (below). Moreover, the nasal septum derives from neural crest cells, whereas the ethmoid components ossify in membranes induced by the placode itself. Additionally, the

**Table III.** Summary of Internal Osseous Elements of the Nose and the Likely Function of Each

| Osseous element     | Primordium                | Ossification mode | Soft tissue                                  | Function                                  | Neural projection                 | Neural termination  |
|---------------------|---------------------------|-------------------|--|---|-----------------------------------|---|
| Mesethmoid          | Septum nasi               | Endochondral      | Olfactory epithelium                         | Social/sexual mediation                   | Terminal nerve                    | Main olfactory bulb, accessory olfactory bulb, hippocampus, forebrain median septum |
| Vomer               | Cartilago paraseptalis    | Perichondral      | Vomeronasal epithelium, etc.                 | Social/sexual mediation                   | Vomeronasal nerve, terminal nerve | Accessory olfactory bulb, hippocampus,  |
| Endoturbinial I     | Nasal capsule membrane    | Perichondral      | Olfactory epithelium, respiratory epithelium | Environmental chemo-analysis; respiration | Olfactory nerve                   | Main olfactory bulb: rostral end, rostrolateral surface                             |
| Endoturbinial II    | Nasal capsule membrane    | Perichondral      | Olfactory epithelium                         | Environmental chemo-analysis              | Olfactory nerve                   | Main olfactory bulb: rostroventral surface  |
| Endoturbinial III   | Nasal capsule membrane    | Perichondral      | Olfactory epithelium                         | Environmental chemo-analysis              | Olfactory nerve                   | Main olfactory bulb: ventrolateral surface  |
| Endoturbinial IV    | Nasal capsule membrane    | Perichondral      | Olfactory epithelium                         | Environmental chemo-analysis              | Olfactory nerve                   | Main olfactory bulb: caudoventral surface   |
| Endoturbinial V     | Nasal capsule membrane    | Perichondral      | Olfactory epithelium                         | Environmental chemo-analysis              | Olfactory nerve                   | Main olfactory bulb: ventromedial surface   |
| Ectoturbinals I, II | Nasal capsule membrane    | Perichondral      | Olfactory epithelium                         | Environmental chemo-analysis              | Olfactory nerve                   | Main olfactory bulb: dorsolateral surface   |
| Nasoturbinial       | Lateral edge, tectum nasi | Perichondral      | Olfactory epithelium, respiratory epithelium | Olfaction                                 | Terminal nerve, olfactory nerve   |   |
| Maxilloturbinal     | Pares nasi, inferior edge | Perichondral      | Respiratory epithelium                       | Respiratory water saturation              |                                   |   |

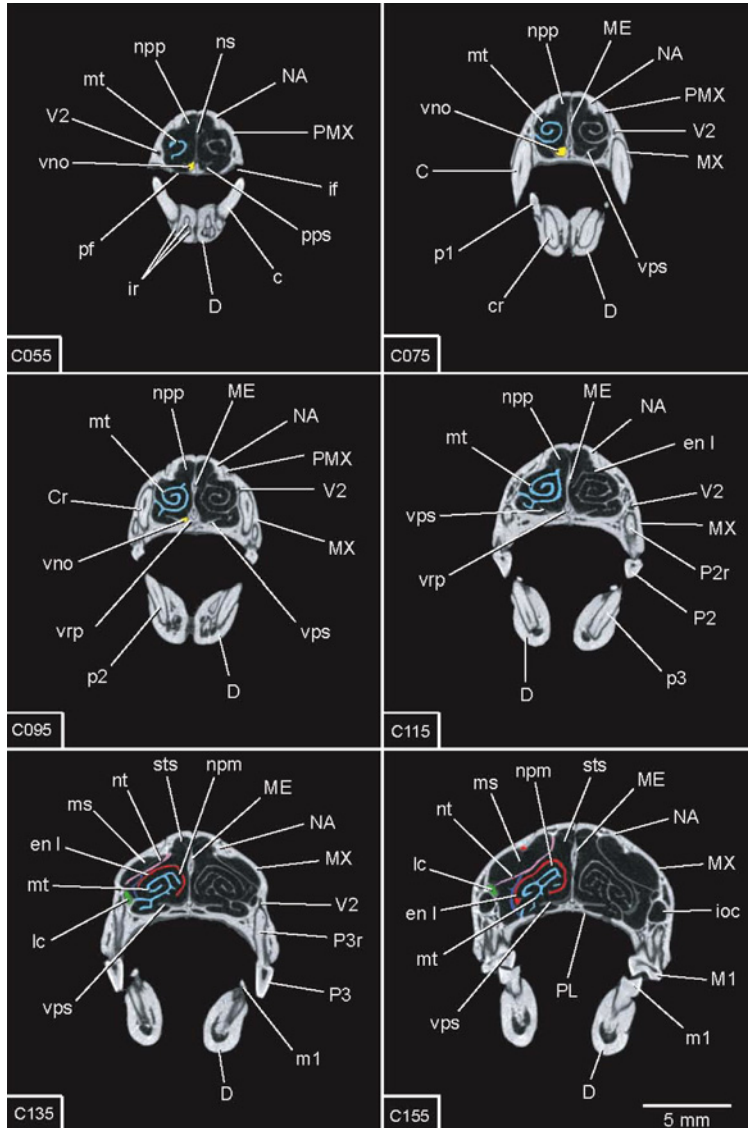


**Fig. 5.** Coronal CT images through the skull of TMM M-7599. Slice numbers are indicated in lower left corner of each image. Turbinals and other ethmoid structures are colored following the convention presented in the text. Scale bar in lower right corner is for all six images. See Appendix I for key to abbreviations.

sensory epithelium covering the mesethmoid is innervated by dendrites of the terminal nerve whereas olfactory nerve dendrites infuse the epithelium covering most of the ethmoidal elements. Lastly, the mesethmoid displays phylogenetic independence from the bilateral ethmoid elements elsewhere among mammals. For example, the mesethmoid and terminal nerve persist in the cetacean *Tursiops*, whereas the bilateral olfactory bulbs, ethmoid turbinals, and cribriform plate are all absent (Ridgway *et al.*, 1987; Colbert *et al.*, 2005).

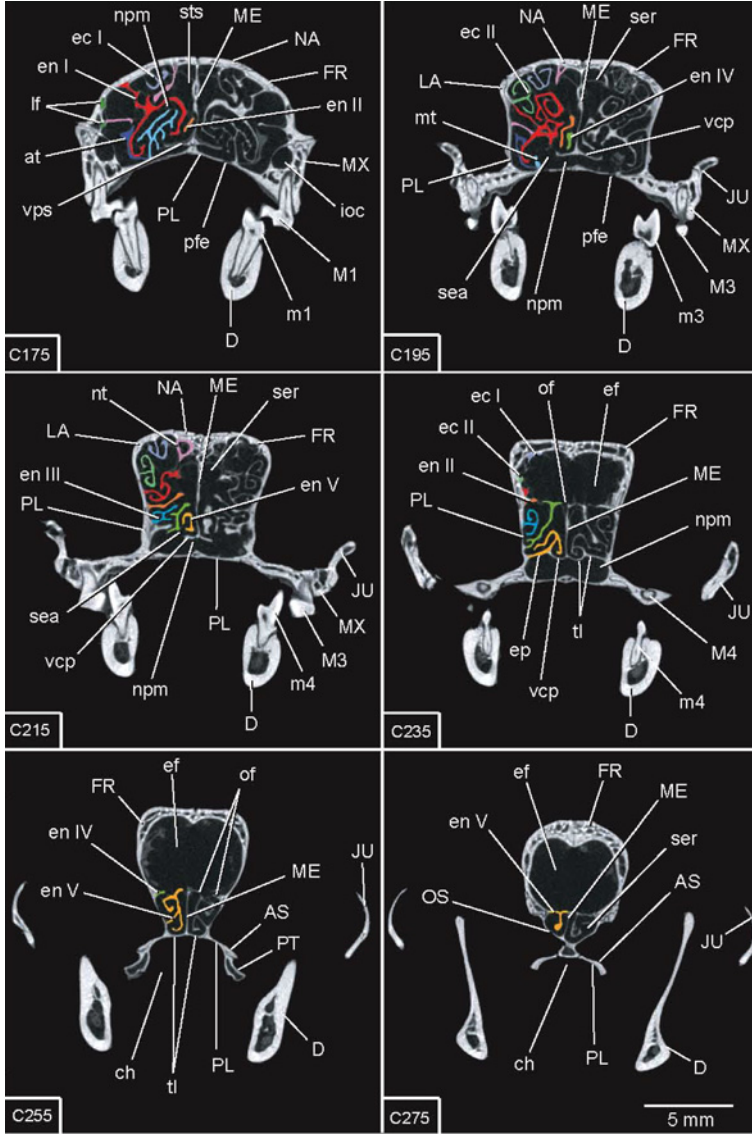


**Fig. 6.** More coronal CT images through the skull of TMM M-7599, see the caption of Fig. 13 for more details. Scale bar in lower right corner is for all six images. See Appendix I for key to abbreviations.

*Bilateral Elements*

*Vomer.* The vomer is a paired bone that extends nearly the entire length of the nose, lying closely applied to the inferior edge of the mesethmoid throughout. Each vomer ossifies from a single perichondral center that arises as a thin sheet of bone appressed to the medial and ventral surfaces of the embryonic paraseptal cartilage.

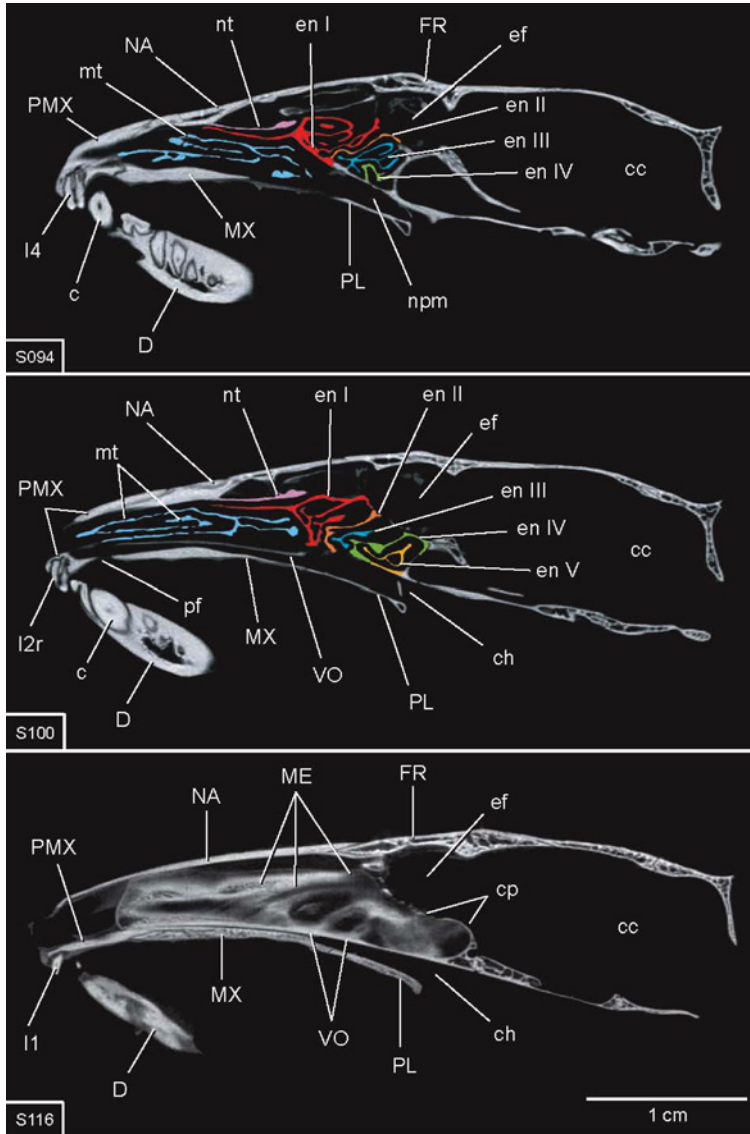


**Fig. 7.** Sagittal CT images through the skull of TMM M-7599. Turbinals are colored following the convention presented in the text. Scale bar is for all three images. See Appendix I for key to abbreviations.

The mature vomer can be divided into distinct rostral and choanal processes. The right and left vomers become fused along the rostral midline early in ontogeny, forming the single median rostral process. The rostral process of the vomer contacts the palatine process of the premaxilla, contributing to the caudal border of the palatine fissure, through which the vomeronasal (Stenson's) duct passes to the roof of the mouth (Fig. 5). The rostral

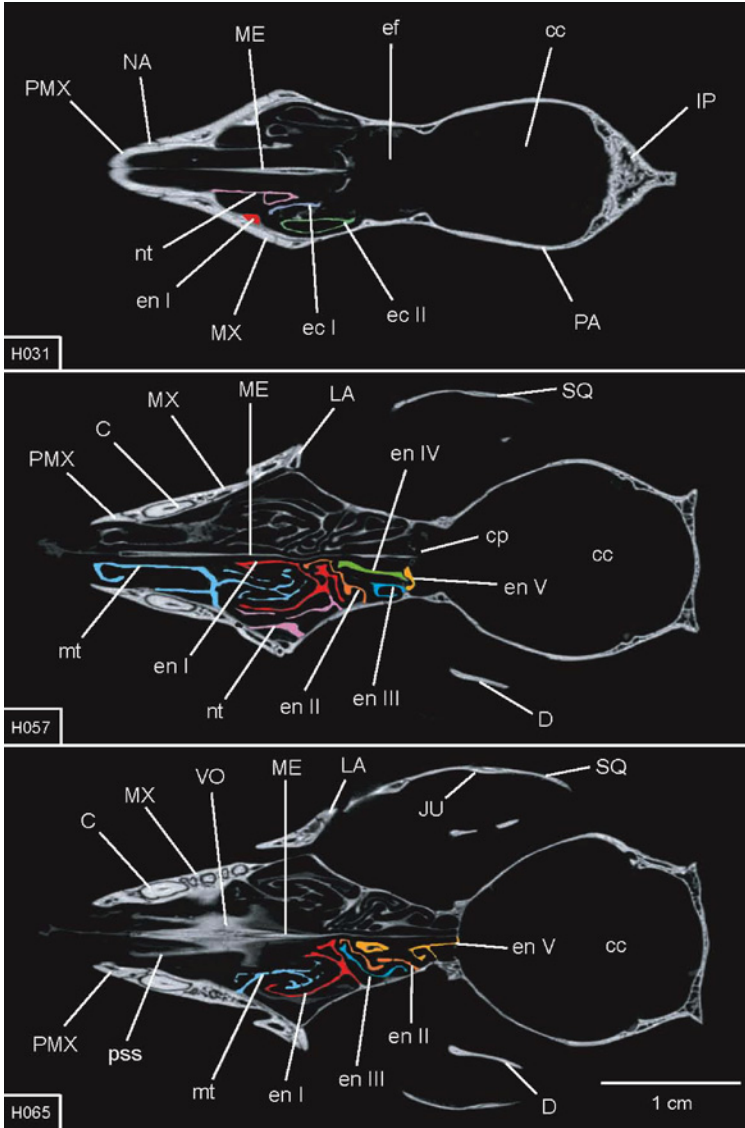


**Fig. 8.** Horizontal CT images through the skull of TMM M-7599. Turbinals are colored following the convention presented in the text. Scale bar is for all three images. See Appendix I for key to abbreviations.

process lies above the median suture between the right and left maxillae, articulating atop a longitudinal prominence developing along the midline suture (Figs. 5 and 8). The superior edge of the rostral process is incised by a V-shaped median groove that holds the inferior edge of the mesethmoidal septum, and also conveys the nasopalatine nerve and vessels. The rostral process completely excludes the mesethmoid from contact with the maxilla and palatine.

The vomer expands laterally into the lumen of the nasopharyngeal passageway as a wing-like paraseptal shelf (Fig. 8). The paraseptal shelf is a compound structure originating in the palatine process of the premaxilla, and continuing caudally as part of the vomer. In *Monodelphis*, the vomeronasal organ lies in a trough along the dorsum of the paraseptal shelf, alongside the base of the mesethmoid, where it is completely enclosed by overlying mucosa and thus isolated from the nasopharyngeal space (Figs. 4, 5 and 9). The inferior surface of the paraseptal shelf is mostly covered by a thin stratified epithelium. The paraseptal shelf flares broadly into the lumen of the nasopharyngeal meatus, forming a partial roof above the floor of the nose. This roof extends along a trough into which the lacrimal duct opens rostrally, and which empties caudally into the choana.

The caudal halves of the vomers remain unfused, where they form choanal processes that extend over the choanal roof from the point where the right and left nasopharyngeal meati become confluent. There, they also join the ethmoid plate to form the transverse lamina (below; Fig. 8). The inferior surface of the transverse lamina contributes to the roof of the choana, while its superior surface forms the floor of the sphenethmoid recess. The sphenethmoidal or superior surface is covered with olfactory epithelium while the inferior or choanal surface is covered by a thin respiratory epithelium.

*Ethmoid.* We describe collectively under the term “ethmoid” a paired complex that develops from separate bilateral ossifications known as turbinals (Owen, 1854), which originate in the epithelium lining the nasal capsule and grow into its lumen. The maxilloturbinal and nasoturbinal attach to their namesake bones in mature specimens, but this attachment is secondary and like other ethmoidal ossifications they arise from ossifications in the lining of the nasal capsule. The nasoturbinal and maxilloturbinal are often considered as elements separate from the “ethmoid.” However, they resemble the other ethmoid elements in arising from the membranous lining of the nasal capsule before eventually fusing to the overlying bones that make up the external skeleton of the nose. We recognize this organizational hierarchy in a hierarchical anatomical nomenclature (Rowe, 1986) in which the adult ethmoid comprises nine individual turbinals in *Monodelphis domestica*. These are the five endoturbinals, two ectoturbinals, the maxilloturbinal, and the nasoturbinal (Figs. 5–8; Tables II and III). Their bases coalesce to varying degrees in adults, forming the cribriform plate and spreading over the inner surfaces of the bones of the outer skeleton of the nose, which renders precise boundaries difficult to trace in mature specimens. We follow other researchers in employing numbers to individuate endoturbinals and ectoturbinals. Each numbered turbinal maintains a strong degree of bilateral symmetry and shows relatively little individual variation between specimens. Bilateral symmetry is also reported in OR gene expression in the mouse (Ressler *et al.*, 1994; Dreyer, 1998). However, we caution that serial homology poses a difficult problem when comparing numbered elements between different species. For example, *Ornithorhynchus* has three endoturbinals whereas *Tachyglossus* has seven (Paulli, 1900a), and it is unclear which of these correspond to the five in *Monodelphis*, or whether a one-to-one correspondence should be expected.

In *Monodelphis*, ethmoid development begins during the second postnatal week, as folds arise in the nasal capsule epithelium, beginning near the olfactory bulb. Cartilage grows apically into the base of each fold and each turbinal arises as a perichondral ossification which surrounds a separate cartilaginous bud. The bud and its ossification grow into the lumen of the nose and elongate rostrally into a plate, a process that extends over several weeks as the snout elongates and dentition erupts. As each turbinal grows, the leading edge

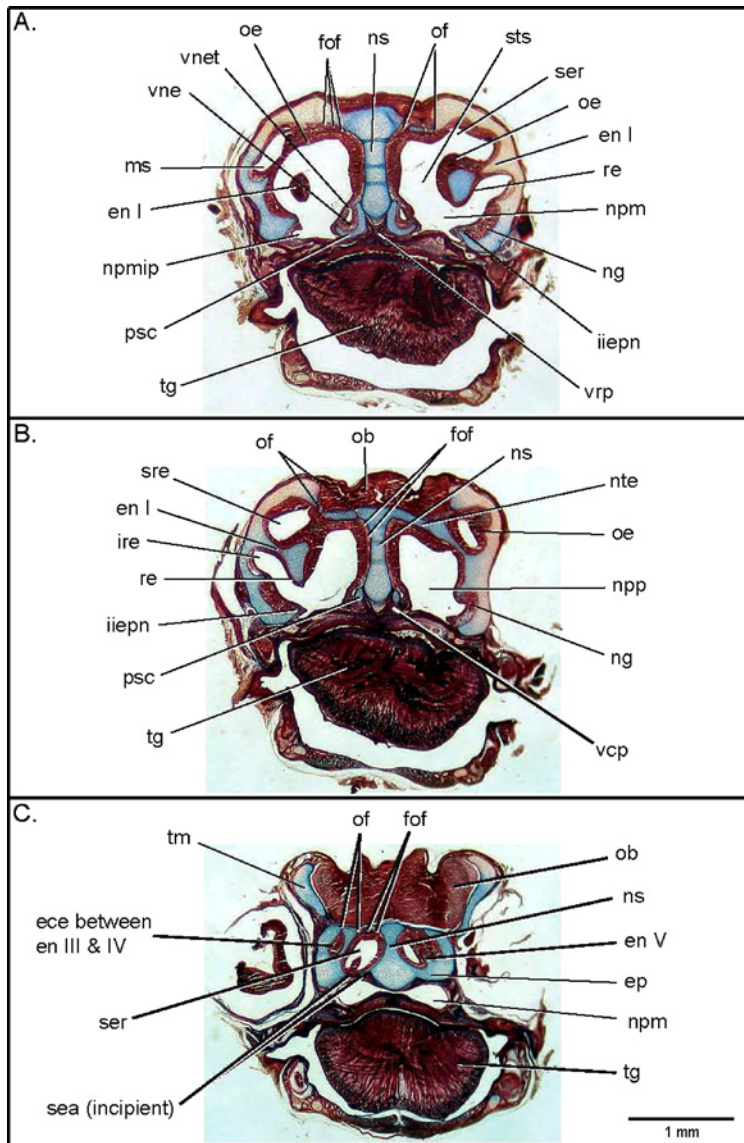


**Fig. 9.** Photomicrograph of coronal histological serial sections through the head of a 10-day-old specimen of *Monodelphis domestica*, stained with azocarmine (for epithelia, connective tissues, nervous tissues) and alcian blue (for cartilage). (A) is taken near rostral extremity of the olfactory bulb and endoturbin I. (B) is taken near caudal extremity of endoturbin I. (C) is taken through the ethmoid cells of the sphenethmoid recess, caudal to endoturbin I. Note that the sections are not precisely orthogonal, and that the side to the reader's left is a few microns rostral to its bilateral counterpart. Also note that the irregular dorsal surface of the olfactory bulb is an artifact of postmortem collapse of the developing brain in sections (B) and (C). Scale bar in lower right corner is for all three images. See Appendix I for key to abbreviations.

of its primary plate may fold or bifurcate into free projecting lobes. The resulting scrolls and arbors of bone fold in upon themselves such that they divide the chamber into narrow passageways. The maxilloturbinal follows the same general pattern as the others, but it arises from a fold at the inferior edge of the wall of the nasal capsule (paries nasi). It is covered entirely by respiratory epithelium and grows from the rostrum in a caudal direction into the nasopharyngeal passage.

*Cribriform Plate.* The cribriform plate is ontogenetically a compound structure that arises from several separate ethmoidal elements that coalesce around the periphery of the olfactory bulbs. The bases of all five endoturbinals and the distal lobes of the ectoturbinals each contribute to the cribriform plate in *Monodelphis*. The cribriform plate forms the wall and floor of the ethmoidal fossa of the endocranial cavity, which holds the olfactory bulbs. At the same time, it forms the roof of the sphenethmoid recess (Fig. 3). The cribriform plate in adults often bears a faintly imbricate structure (Owen, 1854) that reflects the separate origins of its constituent parts.

The numerous olfactory foramina in the cribriform plate form as bone surrounds separate fascicles of olfactory nerve fibers (fila olfactoria), which arise much earlier in ontogeny than the skeleton. Each olfactory foramen, or small cluster of foramina, can be viewed as the terminus of a separate funnel-shaped ethmoid air cell, in which a broad array of OR axons from a distal region of olfactory epithelium are funneled toward a particular location on the olfactory bulb. Once the OR axons have passed through the cribriform plate, they pierce the meninges and converge on the target glomeruli where they make their first synapse (Figs. 3, 6 and 9). Olfactory neurons are continually regenerated during ontogeny from olfactory stem cells, and the funnel-like organization of the ethmoid turbinals and the cribriform plate provides for the guidance of new axons from particular regions of olfactory surface to particular areas on the olfactory bulb, throughout ontogeny (below).

The caudal end of the cribriform surface forms a short non-perforate surface above the region of the sphenethmoid recess into which endoturbinal V projects (e.g., H075). The boundary between the cribriform and non-perforated surfaces is at the level of the annular ridge of the frontal, which projects into the circular fissure of the brain that lies between the olfactory bulb and neocortex. The right and left cribriform plates co-ossify medially with the mesethmoid adjacent to the olfactory bulb (Figs. 6 and 7).

*Endoturbinals.* The endoturbinals differ from the other ethmoid elements in several respects. All five endoturbinals coalesce at their bases around the olfactory bulb, forming the roof of the sphenethmoid cavity. Their distal extremities imbricate and coalesce to form the ethmoid plate at the floor of the cavity. The ethmoid plate joins the vomer to form the transverse lamina, which separates the sphenethmoid recess from the nasopharyngeal meatus. Each endoturbinal thus spans the entire height of the sphenethmoid recess. Most significant is endoturbinal I, in that it is the first to appear in development, its complex shape is largely responsible for separating the respiratory from olfactory regions of the nose (below), and it supports both respiratory and olfactory epithelia. Endoturbinals II–V are dedicated to olfactory epithelium that is served by the olfactory nerve.

Each endoturbinal grows into the lumen of the nose and closely approaches the mesethmoid, but a space known as the septoturbinal space remains between the two. It is a conduit for volatile odorant molecules from the naris to the epithelium over the mesethmoid and in the sphenethmoid recess. The inferior edge of each endoturbinal also contributes to the borders of apertures between the nasopharyngeal passage and the sphenethmoid recess.

These are the sphenethmoid apertures (Fig. 4), which are aligned as a series of four openings between the paraseptal shelf of the vomer and ethmoid plate. They lie rostral to where the vomer and ethmoid plate come together in the transverse lamina. The rostralmost aperture lies between the endoturbinals I and II, while the caudalmost lies between endoturbinals IV and V. The sphenethmoid apertures and septoturbinal space are the principal conduits of volatile odorant molecules to the olfactory epithelium of the sphenethmoid recess from the nasopharyngeal passageway, as well as a drainage opening for secretions from the olfactory epithelium.

*Endoturbinal I.* Endoturbinal I (red; Figs. 5–8) is the primary functional organizer of the nose, as it largely separates the respiratory passageway from the olfactory recess. It is the first ethmoid element to appear in ontogeny. As it grows, it develops a broad rostro-ventral surface that is covered by respiratory epithelium and which folds into a partial tube around the developing maxilloturbinal. This face of endoturbinal I forms much of the roof and walls of the nasopharyngeal passageway and directs respiratory air flow over the elaborate surfaces of maxilloturbinal (e.g., C178 and Fig. 10a and b). At maturity, endoturbinal I has a surface area of 354.4 mm<sup>2</sup>, which is largest for any ethmoid turbinal (Table II). The nasopharyngeal surface of endoturbinal I comprises 20.5% of the total respiratory surface. The respiratory component of endoturbinal I is arrayed over approximately 35% of the total area of this element, while the remaining 65% is covered with olfactory epithelium.

Endoturbinal I is the largest and extends furthest rostrally of the five endoturbinals. In the adult it descends into the lumen from near the junction of the maxillary facial process with the frontal and nasal bones. Endoturbinal I bifurcates several times. Its inferior edge has broad participation in bordering the rostral-most sphenethmoid aperture. Olfactory fibers from the surface of endoturbinal I are funneled through foramina in the cribriform plate to the rostralmost and rostrolateral quadrants of the olfactory bulb.

*Endoturbinal II.* Endoturbinal II (orange; Figs. 6–8) is almost entirely unbranched, consisting of little more than a single olfactory plate with a surface area of only 27.1 mm<sup>2</sup>. It has the simplest shape and is the second smallest of all the endoturbinals (Fig. 10c and d). At the level of the cribriform plate, endoturbinal II protrudes almost horizontally from the medial face of the orbital wall of the palatine, near its junction with the orbital process of the frontal. From back to front, its root migrates rostroventrally, as its olfactory plate passes into the lumen of the sphenethmoid recess. Its inferior extremity meets the ethmoid plate of the transverse lamina just caudal to endoturbinal I. Olfactory fibers from the surfaces of endoturbinal II are directed through the cribriform plate along the ventral surface of the olfactory bulb.

*Endoturbinal III.* Endoturbinal III (blue; Figs. 6–8) consists of a short olfactory plate that bifurcates twice. It has the smallest surface of all the endoturbinals (Fig. 10e and f), being only 23.9 mm<sup>2</sup> in area, and it makes a very short contribution to the cribriform plate along the ventrolateral portion of the olfactory bulb. Its root originates high on the palatine and it descends rostroventrally. All of the other endoturbinals more closely approach the mesethmoid at the septoturbinal space than does endoturbinal III. It contacts the ethmoid plate near the lateral lip of the sphenethmoid aperture, and its rostral-most extremity pinches out as a blunt point between the tips of endoturbinals II and IV. Olfactory axons from the surfaces of endoturbinal III perforate the cribriform plate beneath the ventrolateral parts of the olfactory bulb.

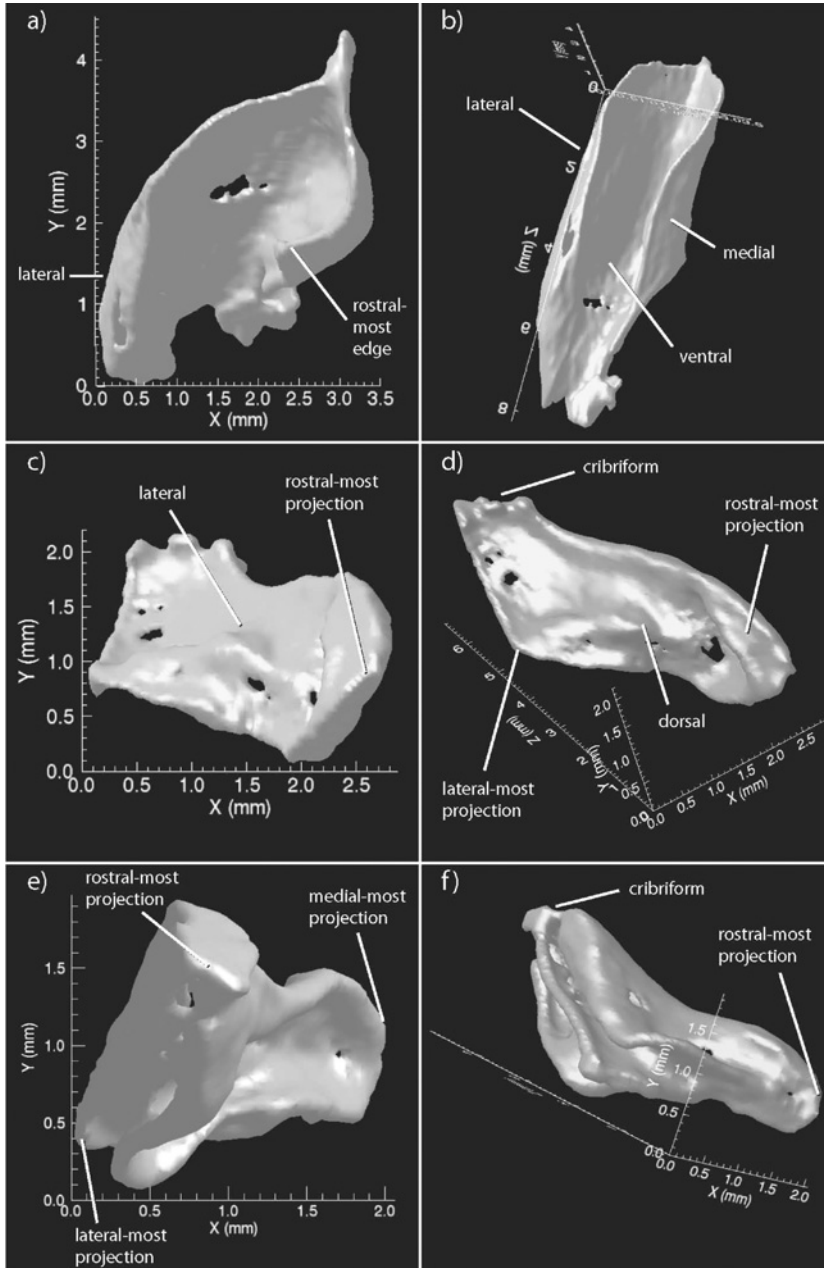


**Fig. 10.** (a) Rostral view of the inferior, crescent shaped branch of Endoturbinale I. (b) Oblique, ventral view of the crescent shaped branch of Endoturbinale I. (c) Rostral view of Endoturbinale II. (d) Oblique, rostrorodorsal view of Endoturbinale II. (e) Rostral view of Endoturbinale III. (f) Rostrolateral view of Endoturbinale III. (a–f) “X”, “Y”, and “Z” refer to sagittal, horizontal, and coronal values, respectively.  $X = 0$  is the lateral-most position in the image;  $Y = 0$  is the ventral-most position in the image, and  $Z = 0$  is the rostral-most position in the image.

*Endoturbinal IV.* Endoturbinal IV (green; Figs. 6–8) originates along the ventral medial surface of the cribriform plate and has a comparable surface to endoturbinals II and III, being 28.8 mm<sup>2</sup>. Its root descends rostroventrally along the inner face of the palatine, ventral to the root of endoturbinal III. It bears three minor bifurcations that are no more than low ridges; it is scarcely more complex than endoturbinal II (Fig. 11a and b). Its rostral extremity pinches out as a blunt point in the sphenethmoid aperture, between endoturbinal II and the mesethmoid. Its epithelium directs axons toward olfactory foramina in the cribriform that lie below the medial part of the caudoventral surface of the olfactory bulb.

*Endoturbinal V.* Endoturbinal V (yellow; Figs. 6–8) is the caudal-most of the endoturbinals and has the second largest surface, being 48.9 mm<sup>2</sup>. It consists of a single olfactory plate, which contacts the medial orbitosphenoid face. The surface area of endoturbinal V is less than half that of endoturbinal I, but nearly twice that of endoturbinals II, III, or IV. It supports the olfactory epithelium that is the most remotely sequestered within in the sphenethmoid recess. The rostral end of endoturbinal V projects toward the caudal-most sphenethmoid aperture and pinches out as a blunt point between endoturbinal IV and the mesethmoid. Its main olfactory plate branches once and the lobes spiral inwards (Fig. 11c and d). Its olfactory fibers are directed through olfactory foramina in the cribriform plate lying along the ventromedial surface of the olfactory bulb, near the caudal extremity of the bulb.

*Ectoturbinals.* The ectoturbinals (I is lavender; II is light green; Figs. 6 and 8) co-ossify as parts of the cribriform plate, forming its dorsolateral wall. However, in contrast to the endoturbinals, they do not meet the transverse lamina, and they remain widely separated from the mesethmoid, hence their designation as ectoturbinals (Allen, 1882). In *Monodelphis* there are two ectoturbinals, each consisting of an olfactory plate that bifurcates once and coils in upon itself (Fig. 12a–d). Ectoturbinal I has a surface area of 43.3 mm<sup>2</sup>, while ectoturbinal II is smaller at 38.6 mm<sup>2</sup>. Both ectoturbinals lie lateral to the olfactory bulbs in the superior recess. This recess lies beneath the frontal and is bounded laterally by both the maxilla and the base of endoturbinal I. Olfactory axons from epithelia covering the ectoturbinals converge on the dorsolateral quadrant of the olfactory bulb. In this respect, and in their peripheral attachment, the ectoturbinals are most intimately associated with endoturbinal I.

*Maxilloturbinal.* The maxilloturbinal (light blue; Figs. 5–8) is covered entirely by respiratory epithelium and it occupies a respiratory passageway known as the nasopharyngeal meatus (Fig. 5c and d), which comprises nearly 45% of the volume (bilateral volume  $\approx 144$  mm<sup>3</sup>) of the nose (Table II). Within this space the maxilloturbinal has a surface area of 183.1 mm<sup>2</sup>, which is six times the surface area of a volume-equivalent sphere, and it supports roughly one-third of the total respiratory epithelium.

The maxilloturbinal differs from other ethmoidal ossifications in several respects. It arises in ontogeny from the rostrum and it grows caudally into the nasopharyngeal meatus. It coils into the lumen of the nasal cavity from the inflected inferior edge of the lateral wall of the embryonic nasal capsule. This contrasts with the other ethmoidal ossifications, which arise adjacent to the olfactory bulb, and grow from the bulb in a rostral direction.

The adult maxilloturbinal is the longest of all the turbinal elements, extending nearly the entire length of the nasopharyngeal meatus (Fig. 11e and f). The rostral tip of its basal plate attaches at a level high on the inner wall of the premaxillary facial process. The free edge of its plate coils dorsally inwards upon itself into the lumen of the nasal cavity.

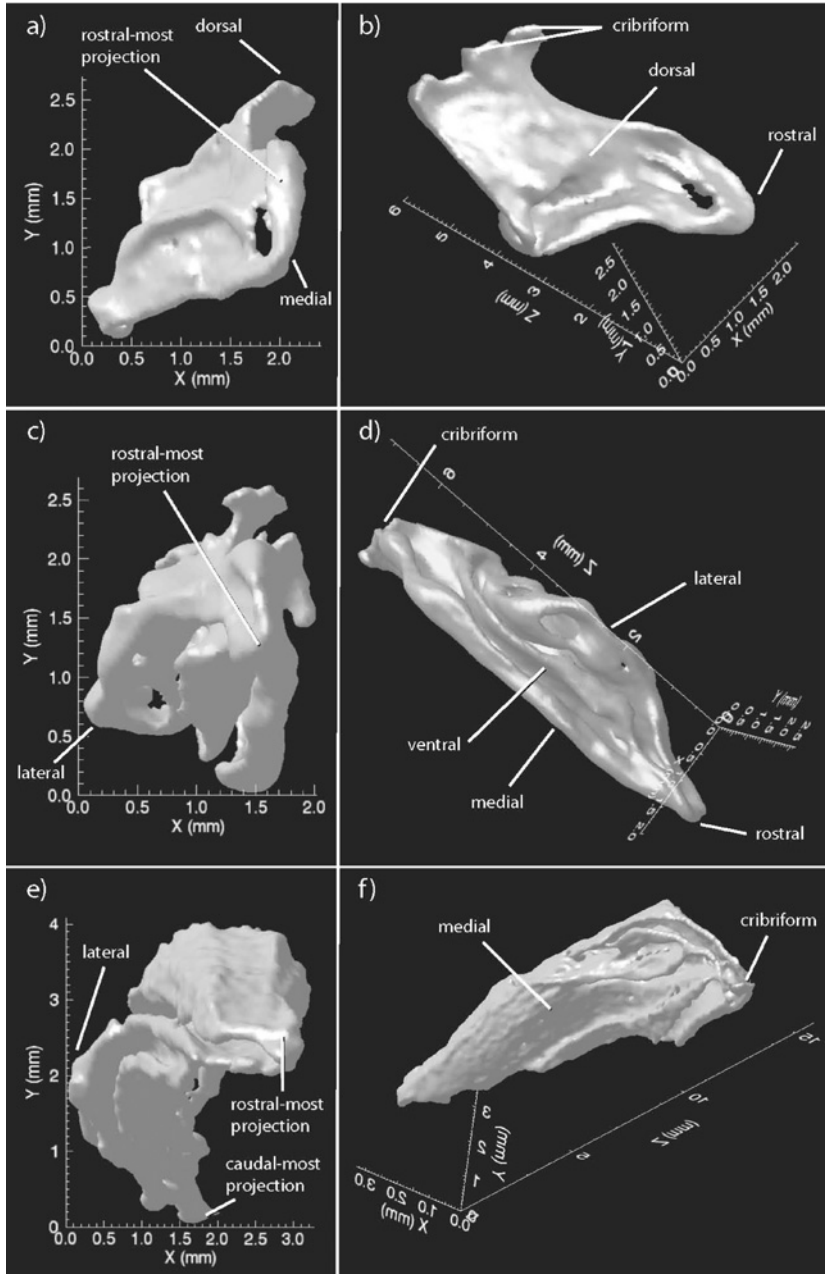


**Fig. 11.** (a) Rostral view of Endoturbinale IV. (b) Oblique, rostradorsal view of Endoturbinale IV. (c) Rostral view of Endoturbinale V. (d) Oblique, ventral view of Endoturbinale V. (e) Rostral view of the Maxilloturbinal. (f) Oblique, posteromedial view of the Maxilloturbinal. (a–f) “X,” “Y,” and “Z” refer to sagittal, horizontal, and coronal values, respectively.  $X = 0$  is the lateral-most position in the image;  $Y = 0$  is the ventral-most position in the image, and  $Z = 0$  is the rostral-most position in the image.

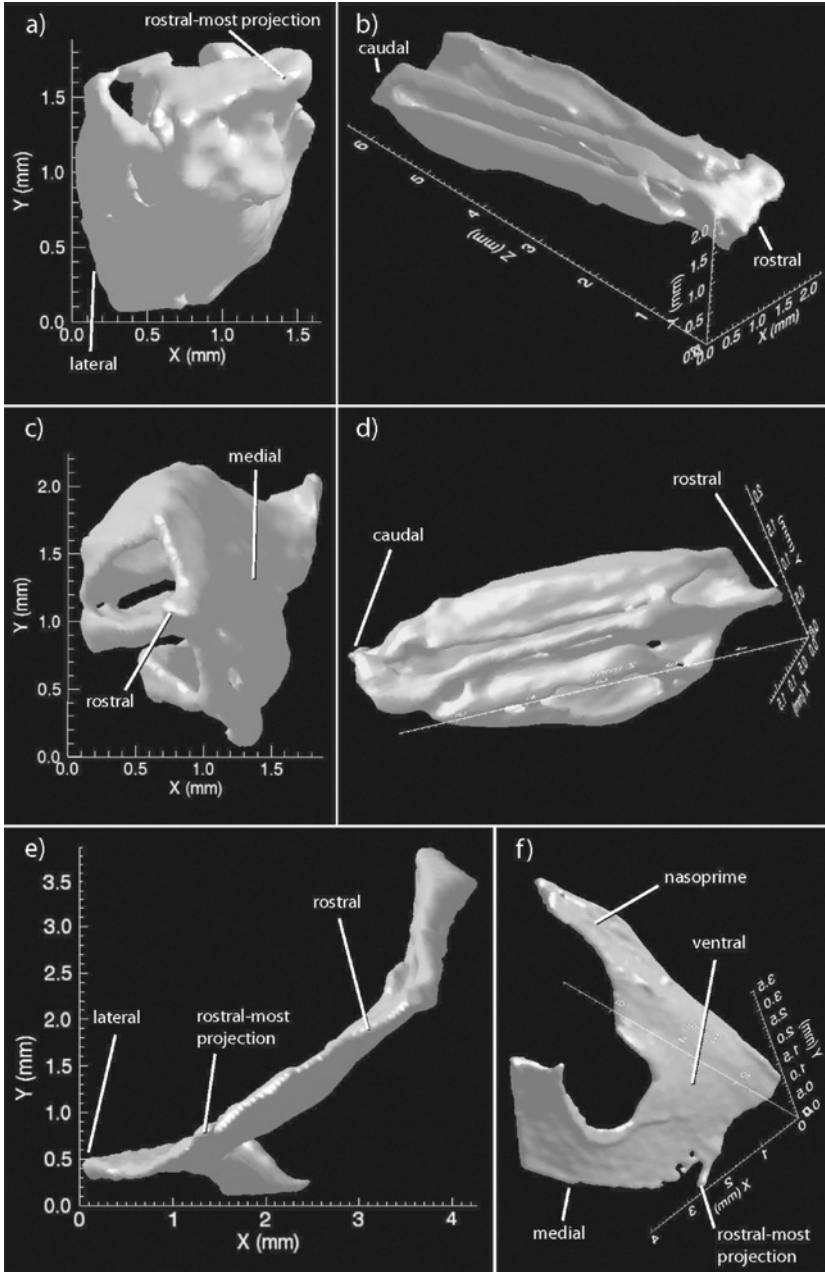


**Fig. 12.** (a) Rostral view of Ectoturbinal I. (b) Oblique, dorsolateral view of Ectoturbinal I. (c) Rostral view of Ectoturbinal II. (d) Oblique, posterolateral view of Ectoturbinal II. (e) Rostral view of Nasoturbinal. (f) Oblique, posteroventral view of Nasoturbinal. (a–f) “X,” “Y,” and “Z” refer to sagittal, horizontal, and coronal values, respectively.  $X = 0$  is the lateral-most position in the image;  $Y = 0$  is the ventral-most position in the image, and  $Z = 0$  is the rostral-most position in the image.

The maxilloturbinal branches into separate lobes caudally, at the level at which it comes to underlie the rostral extremity of endoturbinal I. Its basal junction with the wall of the nasal capsule spirals ventrally over the maxilla and it passes onto the superior face of the palatine palatal shelf, ending at the rostral end of the palatal vacuity. Over its course, it passes over a delicate bony tube built by the maxilla that conveys the nasolacrimal duct. The maxilloturbinal arbor is most extensively branched near its caudal terminus.

*Nasoturbinal.* The nasoturbinal (pink; Figs. 5–8) is among the smaller turbinals, with a surface area of only 28.7 mm<sup>2</sup>. It grows from the dorsolateral edge of the tectum nasi, and extends rostrally to the maxilla, which it joins at a level behind the apex of the canine root. The adult nasoturbinal attaches along the inferior surface of the nasal bone and then divides around the stem of endoturbinal I. Its broad ventral ramus attaches to the maxilla, and a lateral division attaches to the lacrimal and palatine. It forms a broad sheet of bone but never develops the degree of distal elaboration of some of the other olfactory turbinals (Fig. 12e and f).

The nasoturbinal is primarily responsible for enclosing the paranasal sinus complex in mammals. The literature generally claims that there are no paranasal pneumatic sinuses in marsupials, except for *Phascolarctos* (e.g., Moore, 1981; Wible, 1991), a view tracing back to Paulli (1900a). Nonetheless, a shallow facial sinus complex is present throughout postnatal ontogeny in *Monodelphis*, and may be apomorphic for mammals generally (Rowe, 1988). It develops as an invagination into the lateral wall of the cartilaginous nasal capsule and is lined with glandular tissue (Table III). The sinus is relatively much larger in early ontogeny than in adults. The maxillary sinus (C127-159 on right side) forms a blind pocket that lies medial to P3-M1, at a level above the tips of their roots. The maxillary sinus is bounded dorsolaterally by the facial process of the maxilla, dorsomedially by an elongate slip of the nasal, and medially by a thin plate from the nasoturbinal. It communicates with the nasopharyngeal passageway at the level of the distal roots of M1. Caudally, the maxillary sinus is divided by the root of endoturbinal I into a separate superior recess, which contains the two ectoturbinals, and an inferior recess containing glandular tissue.

The proximal nasoturbinal surface, like the mesethmoid, forms a surface over which fila of the terminal nerve are spread. The surface of the nasoturbinal that faces into the nasal lumen is predominantly covered by olfactory epithelium, while the walls that bound and face into the superior recess and the maxillary sinus are covered by respiratory mucosa.

#### *Other Contents of the Nose*

The internal skeleton of the nose is structural and supports several different soft tissues. Thus, a brief consideration of these soft structures offers further insight into the organization of the skeleton.

*Respiratory Epithelium.* The respiratory lining of the nose mediates water and heat exchange, and its basic structure seems uniform among mammalian species studied (Negus, 1958; Schmidt-Nielsen *et al.*, 1970; Bloom and Fawcett, 1975; Hillenius, 1992). Histological sections indicate that in *Monodelphis* this epithelium is supported by the maxilloturbinal, the inferior surface of endoturbinal I, and part of the nasoturbinal (Figs. 9 and 13a,b). Only among the secondarily aquatic cetaceans are the respiratory turbinals secondarily lost (Harrison, 1972; Moore, 1981; Colbert *et al.*, 2005). In *Monodelphis*, approximately 36% of the internal surface area within the nose is covered by respiratory epithelium (Table II),

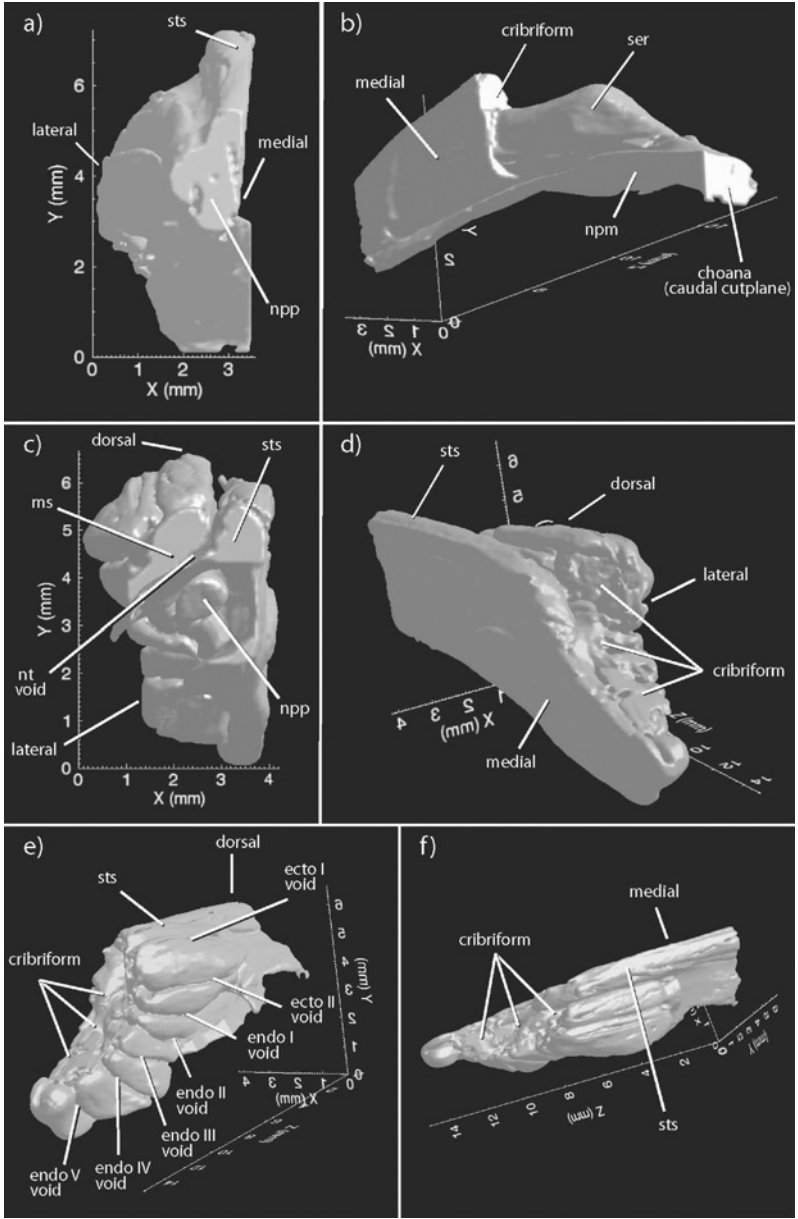


**Fig. 13.** 3-D surface visualization of an endocast of the right nasal cavity, in six views. Voids are the spaces occupied by bony structures (e.g., ecto I void is occupied by the ectoturbinal I). (a) Rostral view of the internal volume of the respiratory chamber. (b) Oblique, caudomedial view of the respiratory chamber. (c) Rostral view of the internal olfactory passage. (d) Oblique, posterior view of the olfactory passage. (e) Posterolateral view of the olfactory passage. (f) Oblique, dorsal view of the olfactory passage. (a–f) “X,” “Y,” and “Z” refer to sagittal, horizontal, and coronal values, respectively.  $X = 0$  is the lateral-most position in the image;  $Y = 0$  is the ventral-most position in the image, and  $Z = 0$  is the rostral-most position in the image. See Appendix I for key to abbreviations.

and the turbinals increase respiratory surface area by 50% over that of the surface of the inner walls of the nasopharyngeal meatus alone.

The epithelium is squamous rostrally, where the integument extends into the nasal vestibule. Downwind of the vestibule, the remainder of the nasopharyngeal meatus is lined with respiratory epithelium that is made up of mucus secreting goblet cells interspersed within ciliated columnar cells. Beneath the epithelium is a venous plexus capable of engorgement, which may serve to both warm and moisten inspired air (Bloom and Fawcett, 1975). In the lungs, air moisture reaches levels near saturation. Experiments on dogs have shown that 75–80% of this moisture in expired air is recovered by the respiratory mucosa in the nose (Goldberg *et al.*, 1981). Evaporative cooling from the respiratory epithelium is also implicated in selective cooling of parts of the brain (Mitchell *et al.*, 2002).

*The “Main” or “Volatile” Olfactory Epithelium.* Discrimination of volatile odorants is initiated by bipolar OR neurons which grow in the olfactory epithelium of the nose (Ressler *et al.*, 1993, 1994). The olfactory epithelium covers approximately 64% of the total surface area inside the nose, and it is distributed over the mesethmoid, all five endoturbinals, and both ectoturbinals. This armature increases the area of olfactory epithelium by a factor of six over that of the enclosing walls alone (Table II).

The olfactory epithelium includes olfactory neurons, glial-like and columnar supporting cells, olfactory stem cells, mucus-secreting cells and Bowman’s glands, which keep the olfactory epithelium moist and which provide a solvent between odorant molecules and olfactory receptors (Bloom and Fawcett, 1975). Olfactory neurons are short-lived cells that are continuously replaced from underlying stem cells (Ressler *et al.*, 1993, 1994). New neurons are also continually generated in the forebrain subventricular region, from which they migrate tangentially and rostrally toward the olfactory bulb (Gheusi *et al.*, 2000; Dreyer, 1998).

Each neuronal cell body projects a single dendrite into a thin surface of mucus that covers the epithelium. Volatile odorant molecules diffusing into the nose bind with ORs covering non-motile cilia-like projections from the distal surfaces of the dendrite. The odorant discriminatory capability in the mouse relies on 913 different OR types, which can be grouped into subfamilies that may recognize different structural classes of odorant molecules (Ressler *et al.*, 1993; Touhara *et al.*, 1999; Ma and Shepherd, 2000; Godfrey *et al.*, 2004).

From each sensory neuron a single axon projects to the brain, and it does not synapse until reaching a target glomerulus or brain nucleus. Neurons expressing a particular OR send axons that converge on a single glomerulus (Mombaerts *et al.*, 1996). In the glomerulus, the OR axons meet dendrites of mitral and tufted cells that form the main projection cells from the bulb to higher order olfactory structures (e.g., the pyriform cortex) and other brain systems. The relay system from neuroepithelium to the mitral and tufted cells is modulated by inputs from other parts of the brain (Shipley *et al.*, 1995). An OR axon does not terminate in more than one glomerulus, and each glomerulus receives impulses from a segregated and independent collection of ORs. Physical zones on the olfactory epithelium thus correspond to particular glomeruli (Ressler *et al.*, 1993, 1994; Mori *et al.*, 1999 and Fig. 13c–f). There are an estimated 6–10 million neurons populating the olfactory membrane in the mouse (Firestein, 2001). An estimated 2000 glomeruli are present in its main and accessory olfactory bulbs, and axons that express the same OR gene converge on the same bilateral pair of glomeruli (Ressler *et al.*, 1994; Mombaerts, 1999; Firestein, 2001). Judging from

similarity in their ethmoidal skeletons, these numbers may be good first approximations for the numbers of OR cells and glomeruli in *Monodelphis*.

OR axons from the endoturbinals and ectoturbinals converge to form the olfactory fila and enter the brain as olfactory nerves via olfactory foramina in the cribriform plate (Fig. 3). ORs contributing to the olfactory nerves are sensitive to volatile molecules conveying non-social signals, but may also play a role in social and reproductive mediation (Keverne, 1999).

In contrast, histological sections indicate that the mesethmoid in *Monodelphis* supports olfactory epithelium that histologically resembles the rest of the “main” OR epithelium, but differs functionally. OR axons from olfactory epithelium supported by the mesethmoid converge toward the brain as the terminal nerve, entering the ethmoid fossa through the ethmoid canal, ventromedial to the olfactory bulbs. Embryological observations on a variety of mammals suggest that the terminal nerve dendrites innervate both the nasal septal wall and the vomeronasal organ (Brown, 1987; Demski, 1987), and that the “vomeronasal nerve” and “terminal nerve” form a loose plexus, rather than two fundamentally separate trunks, with a common function. In all mammals studied to date, the terminal nerve was found to convey signals that mediate social and reproductive behaviors much like the VNO. In *Monodelphis*, epithelium contributing axons to the terminal nerve is confined largely to the mesethmoid, whereas the “main” olfactory epithelium mostly covers the bilateral ossifications of the ethmoid. Terminal nerve fibers synapse in the main and accessory olfactory bulbs, the hippocampus, and medial septum of the forebrain (Wirsig and Leonard, 1987; Nieuwenhuys *et al.*, 1998). Lesion experiments in the hamster reveal that both the terminal nerve and vomeronasal organ play basic roles in reproductive behavior (Wirsig and Leonard, 1987).

*Vomeronasal Organ.* In *Monodelphis*, the vomeronasal organ lies along the parasseptal shelf of the vomer. In all mammals and other tetrapods yet studied, the VNO is responsive to soluble high-molecular weight odorant molecules, primarily pheromones (Keverne, 1999; Del Punta *et al.*, 2002; Watson, 1999). For example, one chromatographic analysis isolated a soluble protein (aphrodisin) weighing 17,600 Da, which stimulates copulation in hamsters when introduced to the VNO. As observed in the cat, the outer layer of the VNO is an erectile tissue that functions as a physiological pump (Salazar *et al.*, 1997), possibly to agitate odorant molecules into, and expel them from the blind, fluid-filled lumen.

When well-developed in mammals, the VNO expresses at least two gene families, one consisting of 100 odorant receptor genes, the second of about 40 genes (Dryer, 2000). Like the volatile olfactory system, the VNO epithelium deploys G-protein coupled receptors, but each receptor is expressed in only a few individual neurons, and the epithelium is non-ciliated. The two gene families are expressed in spatially segregated epithelial zones. Neither one shares close sequence similarity to the “main” olfactory OR genes, and the receptor cells themselves are sensitive to a completely different repertoire of soluble molecules (Singer *et al.*, 1987; Dryer, 2000). The VNO genes of *Monodelphis* have yet to be mapped.

In ontogeny, differentiation of the VNO and accessory olfactory bulb lag behind that of the main olfactory epithelium and bulb in *Monodelphis* by about 2 weeks (Shapiro *et al.*, 1997). The VNO axons course over the wall of the mesethmoid and join the terminal nerve as they enter the ethmoid fossa, and project both to the accessory olfactory bulb and toward the hippocampus, but not to the main olfactory bulb. The VNO functions as a chemosensory detector involved in conspecific communication and reproduction in

*Monodelphis domestica* (Poran, 1998). Its ontogenetic and systematic variation among marsupials is described by Sánchez-Villagra (2001).

*Nasal Gland.* The nasal gland occupies nearly 20% of the total volume of the nasopharyngeal chamber in *Monodelphis*, and it is a major producer of mucous. It lies in a space that communicates at either end with the nasopharyngeal passageway (Fig. 9). The nasal gland is enclosed laterally by the facial process of the maxilla, in a position caudal to the upper canine root. The upper boundary of this space is formed as the rostral plate of the nasoturbinal joins the inner surface of the maxilla. The lower border of the nasal gland recess is bounded by the stem of the maxilloturbinal. The medial surface of the nasal gland is covered by thick connective tissue that in dried skulls resembles a bony turbinal, the “atrioturbinal” (Toeplitz, 1920; dark purple on CT images), but does not ossify in *Monodelphis*.

*Penetrations.* The orbital wall is perforated by three openings of the lacrimal duct, which drain lacrimal gland and Harder’s gland fluids from the orbit, through a downward sloping lacrimal canal (Figs. 5 and 6). This canal is enclosed by the maxilla in a thin-walled tube that empties near the floor of the rostral nasopharyngeal meatus. Also perforating the orbital wall are branches of cranial nerves V and VII, the maxillary artery, and other vessels supplying the inner tissues of the nose.

## DISCUSSION

A fundamental factor in the origin of mammals and diversification of mammalian life history strategies involved enhanced sensitivity and resolution in the detection, identification, and source location of volatile airborne odorant molecules. The vomeronasal organ was probably well-developed in mammals ancestrally (Butler and Hodos, 1996; Nieuwenhuys *et al.*, 1998), and sensitivity to soluble odorants has remained important throughout the histories of most mammalian clades. But sensitivity to soluble odorants is plesiomorphic for mammals, while in the process of adapting to a “smellscape” (Watson, 1999) of volatile odors, mammals acquired an order of magnitude more OR genes than has yet been measured in any other chordate. Throughout its subsequent history, the mammalian olfactory system continued to evolve in a rapid and complex pattern that involved transformations in the number of active OR genes and extensive rearrangements among the chromosomes harboring OR genes (Niimura and Nei, 2003); elaboration of the olfactory bulb and neocortex (Nieuwenhuys *et al.*, 1998; Rowe, 1988, 1993, 1996a,b); and variation of the architecture of the internal skeleton of the nose (Paulli, 1900a,b,c).

One of the most intriguing aspects of this skeleton is that it has adapted to fill the confines of the nasal cavity without having radically altered the overall shape of the snout. This may reflect a developmental constraint imposed by the dentition. Virtually all mammals and their proximal extinct relatives have teeth with elongated roots, cheek teeth with multiple roots, reduced dental replacement rates, and an occlusal relationship between upper and lower teeth. Many features of this apparatus and its geometric organization in *Monodelphis* phylogenetically preceded the appearance of an ossified ethmoid complex (Rowe, 1988, 1993, 2004). Additionally, phylogenetic variability of the masticatory system within mammals seems largely independent of changes occurring to the skeleton inside the nose, although it is hard to predict what patterns and correlations may emerge should the mammalian ethmoidal skeleton become as well studied as the dentition.

A glimpse of the historic complexity of the mammalian olfactory system can be seen in comparing mouse and human. The mouse has approximately 2.7 times as many ORs as humans but only 1.4 times as many subfamilies (Godfrey *et al.*, 2004; Malnic *et al.*, 2004). Numerous subfamilies are shared by the two species, but in most cases (89%) the number of ORs in a shared subfamily is greater in mouse than in human (Godfrey *et al.*, 2004). The number of subfamilies has been suggested as a predictor of the diversity of odorant features a species can detect (Godfrey *et al.*, 2004). It appears that intact human genes are found in most OR subfamilies, which means that humans may be able to detect as wide a range of odorants as mice, but mice may be more sensitive to odors and better able to distinguish closely related odors (Kay *et al.*, 2004). Mice also have a much more extensive turbinal system than humans; hence the surface area of olfactory epithelium, the degree of olfactory placation may be predictors of sensitivity and/or resolution. If that is the case, the architectural complexity seen in the internal skeleton of *Monodelphis* and *Mus* is considerably less than that seen in at least some other mammals, such as *Tachyglossus* and *Zaglossus*. On this basis, they might be predicted to have more than the 1000 OR functional genes reported in the mouse, and to have the “best” of mammal noses. This too remains speculative, however, insofar as the olfactory genome is known at present in only a few mammal species.

Axonal guidance is also problematic (Mombaerts, 1999; Mori *et al.*, 1999; Dryer, 2000) in that experimental data have been unable to identify an extrinsic guidance mechanism for the axons of olfactory neurons. New olfactory neurons arise in olfactory epithelium throughout ontogeny and their axons must successfully find their proper target glomerulus in the olfactory bulb. In *Monodelphis*, a new peripheral axon may travel distances up to 10's of millimeters before reaching this target, and the internal skeleton of the nose may play an important role in funneling axons into close approximation to their intended target. The olfactory bulbs and epithelium are induced as the olfactory placodes contact the rostral end of the forebrain in early ontogeny (Hall, 1990; Noden, 1990), and thus a connection between the two tissues is begun from their time of differentiation. The epithelium growth reflects the underlying geometry of skeletal growth, such that the epithelium lines the mouths of numerous widening funnels, forming the blind ethmoid cells into which volatile odorants diffuse. The neck of each funnel “empties” OR neuron axons through one or a very few olfactory foramina in the cribriform plate, delivering each new axon to the same locale as its predecessor at the olfactory bulb, while other mechanisms are involved in axonal targeting of specific glomeruli once the axon contacts the brain (Berlingrood, 1969). Skeletal geometry may play an important role in delivering the growing axon tips very close to their primary synaptic targets in the brain.

The nature of the peripheral olfactory code may also be influenced in certain regards by the geometry of its supporting olfactory skeleton. It has long been recognized that the topographic organization of the turbinals reflects the underlying organization of the olfactory bulb, but exactly what is being encoded is less certain (Laurent, 1999). Expression of OR genes proceeds as the olfactory neurons multiply and as the olfactory epithelium grows from the olfactory bulb. G-protein coupled ORs detect molecular identity, and the number of ORs and glomeruli recruited reportedly reflects odorant intensity (Rubin and Katz, 1999). The epithelium is organized in zones expressing a small number of OR types, and the distribution of particular OR cells throughout any zone is stochastic rather than clumped. Whereas most models of peripheral coding argue for a combinatorial code,

geometry of the epithelial surface may afford an opportunity to measure the speed at which a bloom of odorant molecules diffuses into a blind “ethmoid cell” and across a particular OR expression zone. Insofar as particular OR types all make their first synapse in a single or small number of glomeruli, a glomerulus may potentially function in temporal signal processing and measuring the volatility of a bloom. If this interpretation is correct, the most elementary attributes encoded at the olfactory epithelium may be molecule-class identity, concentration, and volatility. Other combinatorial aspects of olfaction, such as directionality, enter the cognitive pathway only following their first synapse, in inter- and post-glomerular processing.

An elaborate respiratory skeleton evolved seemingly in concert with the olfactory elements of the ethmoid, with the simultaneous appearance of both an ossified maxilloturbinal and endoturbinal I, the latter element forming a tube that encloses the former and channels air through the “sieve” of the maxilloturbinal. There has been much speculation regarding what the maxilloturbinal may mean in terms of mammalian endothermy. A ridge of attachment for a cartilaginous maxilloturbinal primordium is reported in many non-mammalian therapsids (e.g., Hillenius, 1992). Even so, it is difficult to understand how an isolated maxilloturbinal would work unless endoturbinal I (or its equivalent) was also present to constrain the air passage through the “sieve” of the maxilloturbinal. Despite the speculation, there are no verified reports of fossils representing non-mammalian synapsids which possess an ossified internal respiratory or olfactory skeleton in the nose. At present, the ossification of both the mesethmoid and ethmoid are most simply interpreted as apomorphic conditions of Mammalia (Rowe, 1988, 1993). However, the question of whether intermediate stages were present in panmammalian Mesozoic fossils can now be revisited with HRXCT. Further exploration of this complex skeleton in mammals and their fossil relatives may also provide a promising new source of systematic data and will doubtless reveal an interesting story of olfactory evolution in mammals.

#### APPENDIX: FIGURE ABBREVIATIONS

| Abbreviation | Structure         | Abbreviation | Structure                                |
|--------------|-------------------|--------------|--|
| AS           | Alisphenoid       | lf           | Lacrimal foramina                        |
| at           | “Atrioturbinal”   | m1           | Lower 1st molar                          |
| c            | Lower canine      | M1           | Upper 1st molar                          |
| C            | Upper canine      | m3           | Lower 3rd molar                          |
| cc           | Cranial cavity    | M3           | Upper 3rd molar                          |
| cg           | Crista galli      | m4           | Lower 4th molar                          |
| ch           | Choana            | M4           | Upper 4th molar                          |
| cp           | Cribriform plate  | ME           | Mesethmoid                               |
| cr           | Lower canine root | ms           | Maxillary sinus                          |
| Cr           | Upper canine root | mt           | Maxilloturbinal                          |
| D            | Dentary           | MX           | Maxilla                                  |
| ec I         | Ectoturbinal I    | NA           | Nasal                                    |
| ec II        | Ectoturbinal II   | ng           | Nasal gland                              |
| ece          | Ethmoid cell      | npm          | Nasopharygeal meatus                     |
| ECT          | Ectotympanic      | npmip        | Nasopharygeal meatus<br>inferior passage |
| ef           | Ethmoid fossa     | npp          | Nasopharygeal passageway                 |
| en I         | Endoturbinal I    | ns           | Nasal septum                             |

## APPENDIX: Continued

| Abbreviation | Structure   | Abbreviation | Structure                     |
|--------------|---|--------------|-------------------------------|
| en II        | Endoturbinale II  | nt           | Nasoturbinale                 |
| en III       | Endoturbinale III                                       | nte          | Nasal tectum                  |
| en IV        | Endoturbinale IV  | ob           | Olfactory bulb                |
| en V         | Endoturbinale V   | oe           | Olfactory epithelium          |
| EO           | Exoccipital   | of           | Olfactory foramen             |
| ep           | Ethmoid plate   | OS           | Orbitosphenoid                |
| fo           | Foramen ovale (V3)                                      | p1           | Lower 1st premolar            |
| fof          | Fila olfactoria   | p2           | Lower 2nd premolar            |
| fr           | Foramen rotundum (V2)                                   | P2           | Upper 2nd premolar            |
| FR           | Frontal   | P2r          | Upper 2nd premolar root       |
| hf           | Hypoglossal foramen (XII)                               | p3           | Lower 3rd premolar            |
| hyf          | Hypophyseal fossa                                       | P3           | Upper 3rd premolar            |
| I1           | Upper 1st incisor                                       | P3r          | Upper 3rd premolar root       |
| I2r          | Upper 2nd incisor root                                  | PA           | Parietal                      |
| I4           | Upper 4th incisor                                       | pf           | Palatine fissure              |
| if           | Incisive fossa  | pfe          | Palatal fenestra              |
| iielpn       | Inflected inferior edge of paries nasi                  | PL           | Palatine                      |
| ioc          | Maxillary branch of trigeminal nerve infraorbital canal | PMX          | Premaxilla trigeminal         |
| iof          | Infraorbital foramen                                    | ppp          | Premaxillary palatine process |
| IP           | Interparietal   | pps          | Premaxillary paraseptal shelf |
| ir           | Lower incisor roots                                     | psc          | Paraseptal cartilage          |
| ire          | Inferior recess   | pss          | Paraseptal shelf              |
| JU           | Jugal   | PT           | Pterygoid                     |
| LA           | Lacrimal  | re           | Respiratory epithelium        |
| lc           | Lacrimal canal  | sea          | Sphenethmoid aperture         |
| ser          | Sphenethmoid recess                                     | vcp          | Vomer choanal process         |
| sof          | Sphenorbital fissure                                    | vnd          | Vomer nasal duct              |
| SQ           | Squamosal   | vne          | Vomer nasal epithelium        |
| sre          | Superior recess   | vnet         | Vomer nasal erectile tissue   |
| sts          | Septoturbinale space                                    | vno          | Vomer nasal organ cavity      |
| tg           | Tongue  | VO           | Vomer                         |
| tl           | Transverse lamina                                       | vps          | Vomer paraseptal shelf        |
| tm           | Taenia marginalis                                       | vrp          | Vomer rostral process         |
| V2           | Maxillary branch of trigeminal nerve canal              |              |                               |

## ACKNOWLEDGMENT

This paper is dedicated to Bill Clemens, friend and mentor, who directly or indirectly inspired our interests in mammalian history. We thank John VandeBerg of the Southwest Foundation for Biomedical Research in San Antonio, TX for providing specimens used in this study. CT scanning for this project was funded by National Science Foundation grants IIS 9874781, IIS 0208675 (to TR), and DEB 0309369 (to TM). Development and application of Blob3D software was supported by National Science Foundation grant EAR-0113480

(to RK). Matt Colbert and Julian Humphries assisted with digital image processing and implementation of imagery on the internet. For critical reviews of earlier drafts of this manuscript, we thank Amy Balanoff, Eric Ekdale, Jeri Rodgers, James Sprinkle, Nina Triche, Jon Wagner, Farrah Welch, Larry Witmer, and an anonymous reviewer. Support for this work was provided in part by the John A. and Katherine G. Jackson School of Geosciences and the Geology Foundation at the University of Texas at Austin.

## LITERATURE CITED

- Allen, H. (1882). On a revision of the ethmoid bone in the Mammalia. *Bull. Mus. Comp. Zool.* **10**: 135–164.
- Berlingrood, M. (1969). *A Study of the Outgrowth and Pathway Determination of Nerve Fibers in the Newt*, Ph.D. Dissertation, The University of Texas at Austin.
- Bloom, W., and Fawcett, D. W. (1975). *A Textbook of Histology*, 10th Ed., W. B. Saunders Company, Philadelphia.
- Brown, J. W. (1987). The nervus terminalis in insectivorous bat embryos and notes on its presence during human ontogeny. *Ann. N. Y. Acad. Sci.* **519**: 174–183.
- Buck, L., and Axel, R. (1991). A novel multigene family may encode odorant receptors: A molecular basis of odor recognition. *Cell* **65**: 175–187.
- Butler, A. B., and Hodson, W. (1996). *Comparative Vertebrate Neuroanatomy*, Wiley, New York.
- Carlson, W. D., Rowe, T., Ketcham, R. A., and Colbert, M. W. (2003). Geological applications of high-resolution X-ray computed tomography in petrology, meteoritics and palaeontology. In: *Applications of X-ray Computed Tomography in the Geosciences, Vol. 215*, F. Mees, R. Swennen, M. Van Geet, and P. Jacobs, eds., pp. 7–22, Geological Society, London.
- Clark, C. T., and Smith, K. K. (1993). Cranial osteogenesis in *Monodelphis domestica* (Didelphidae) and *Macropus eugenii* (Macropodidae). *J. Morphol.* **215**: 119–149.
- Cleland, J. (1862). On the relations of the vomer, ethmoid, and intermaxillary bones. *Phil. Trans. R. Soc. Lond.* **152**: 289–321.
- Colbert, M. W., Racicot, R., and Rowe, T. (2005). Anatomy of the cranial endocast of the bottlenose dolphin *Tursiops truncatus*, based on HRXCT. *J. Mamm. Evol.* **12** (in press).
- Coues, E. (1872). On the osteology and myology of *Didelphis virginiana*. *Mem. Boston Soc. Nat. Hist.* **2**: 41–154.
- De Beer, G. R. (1937). *The Development of the Vertebrate Skull*, Oxford University Press, Oxford.
- Del Punta, K., Leinders-Zufall, T., Rodriguez, I., Jukam, D., Wysocki, C. J., Ogawa, S., Zufall, F., and Mombaerts, P. (2002). Deficient pheromone responses in mice lacking a cluster of vomeronasal receptor genes. *Nature* **419**: 70–74.
- Demski, L. S. (1987). Phylogeny of luteinizing hormone-releasing hormone systems in protochordates and vertebrates. *Ann. N. Y. Acad. Sci.* **519**: 1–14.
- Ducham-Viret, P., Chaput, M. A., and Duchamp, A. (1999). Odor response properties of rat olfactory receptor neurons. *Science* **284**: 2171–2174.
- Dreyer, W. (1998). The area code hypotheses revisited: Olfactory receptors and other related transmembrane receptors may function as the last digits in a cell surface code for assembling embryos. *Proc. Natl. Acad. Sci. U.S.A.* **95**: 9072–9077.
- Dryer, L. (2000). Evolution of odorant receptors. *BioEssays* **22**: 803–810.
- Firestein, S. (2001). How the olfactory system makes sense of scents. *Nature* **413**: 211–218.
- Gauthier, J., Kluge, A. G., and Rowe, T. (1988). Amniote phylogeny and the importance of fossils. *Cladistics* **4**: 105–209.
- Gheusi, G., Cremer, H., McLean, H., Chazal, G., Vincent, J.-D., and Lledo, P.-M. (2000). Importance of newly generated neurons in the adult olfactory bulb for odor discrimination. *Proc. Natl. Acad. Sci. U.S.A.* **97**: 1823–1828.
- Godfrey, P. A., Malnic, B., and Buck, L. B. (2004). The mouse olfactory receptor gene family. *Proc. Natl. Acad. Sci. U.S.A.* **101**: 2156–2161.
- Goldberg, M. B., Langman, V. A., and Taylor, C. R. (1981). Panting in dogs: Paths of air flow in response to heat and exercise. *Respir. Physiol.* **43**: 327–338.
- Gregory, W. K. (1910). The orders of mammals. *Bull. Am. Mus. Nat. Hist.* **27**: 1–524.
- Hall, B. K. (1990). Tissue interactions in the development and evolution of the vertebrate head. In: *Developmental and Evolutionary Aspects of the Neural Crest*, P. F. A. Maderson, ed., pp. 159–260, Wiley, New York.
- Harrison, R. J. (1972). *Functional Anatomy of Marine Mammals*, Academic Press, London.
- Hillenius, W. J. (1992). The evolution of nasal turbinates and mammalian endothermy. *Paleobiology* **18**: 17–29.

- Kay, R. F., Campbell, V. M., Rossis, J. B., Colbert, M. W., and Rowe, T. B. (2004). The olfactory system of *Tremacebus harringtoni* (Platyrrhini, early Miocene, Cacanana, Argentina): Implications for activity pattern. *Anat. Rec. (A)* **281A**: 1157–1172.
- Ketcham, R. A., and Carlson, W. D. (2001). Acquisition, optimization and interpretation of X-ray computed tomographic imagery: Applications to the geosciences. *Comput. Geosci.* **27**: 381–400.
- Ketcham, R. A. (2005). Computer methods for quantitative analysis of three-dimensional features in geological specimens. *Geosphere* **1**: 32–41.
- Keverne, E. B. (1999). The vomeronasal organ. *Science* **286**: 716–720.
- Lane, R. P., Cutforth, T., Young, J., Athanasiou, M., Friedman, C., Rowen, L., Evans, G., Axel, R., Hood, L., and Trask, B. J. (2001). Genomic analysis of orthologous mouse and human olfactory receptor loci. *Proc. Natl. Acad. Sci. U.S.A.* **98**: 7390–7395.
- Laurent, G. (1999). A systems perspective on early olfactory coding. *Science* **286**: 723–728.
- Ma, M., and Sheppard, G. M. (2000). Functional mosaic organization of mouse olfactory receptor neurons. *Proc. Natl. Acad. Sci. U.S.A.* **97**: 12869–12874.
- Macrini, T. E. (2000). *High Resolution X-ray Computed Tomography (CT) of the Skull of an Extant Opossum (Monodelphis domestica) and a Comparison of its Ontogeny to Synapsid Phylogeny*, Unpublished M. S. Thesis, The University of Texas at Austin, Austin.
- Malnic, B., Godfrey, P. A., and Buck, L. B. (2004). The human olfactory receptor gene family. *Proc. Natl. Acad. Sci. U.S.A.* **101**: 2584–2589.
- Marshall, L. G., and de Muizon, C. (1995). Part II. The skull. In: *Pucadelphys andinus* (Marsupialia, Mammalia) from the early Paleocene of Bolivia, L. G. Marshall, C. de Muizon, and D. Signogneau-Russell, eds., *Mém. Mus. Hist. Nat., Paris* **165**: 21–90.
- Mitchell, E., Maloney, S. K., Jessen, C., Laburn, H. P., Kamerman, P. R., Mitchell, G., and Fuller, A. (2002). Adaptive heterothermy and selective brain-cooling in arid-zone mammals. *Comp. Biochem. Physiol. B Biochem. Mol. Biol.* **131**: 571–585.
- Mombaerts, P. (1999). Seven-transmembrane proteins as odorant and chemoreceptors. *Science* **286**: 707–711.
- Mombaerts, P., Wang, F., Dulac, C., Chao, S. K., Nemes, A., Mendelsohn, M., Edmondson, J., and Axel, R. (1996). Visualizing an Olfactory Sensory Map. *Cell* **87**: 675–686.
- Moore, W. J. (1981). *The Mammalian Skull*, Cambridge University Press, Cambridge, Massachusetts.
- Mori, K., Nagao, H., and Yoshihara, Y. (1999). The olfactory bulb: Coding and processing of odor molecule information. *Science* **286**: 711–715.
- Negus, V. (1958). *The Comparative Anatomy and Physiology of the Nose and Paranasal Sinuses*, Livingstone, Edinburgh.
- Nieuwenhuys, R., Ten Donkelaar, H. J., and Nicholson, C. (1998). *The Central Nervous System of Vertebrates*, Springer, Berlin.
- Niimura, Y., and Nei, M. (2003). Evolution of olfactory receptor genes in the human genome. *Proc. Natl. Acad. Sci. U.S.A.* **100**: 12235–12240.
- Noden, D. M. (1990). Interactions between cephalic neural crest and mesodermal populations. In: *Developmental and Evolutionary Aspects of the Neural Crest*, P. F. A. Maderson, ed., pp. 89–120, Wiley, New York.
- Novacek, M. J. (1993). Patterns of diversity on the mammalian skull. In: *The Skull, Vol. 2*, J. Hanken and B. K. Hall, eds., pp. 438–545, University of Chicago Press, Chicago.
- Owen, R. (1854). *The Principal Forms of the Skeleton and of the Teeth*, Blanchard and Lea, Philadelphia.
- Paulli, S. (1900a). Ueber die Pneumaticität des Schädels bei den Säugethieren. I. Ueber die Morphologie des Siebbeins und die Pneumaticität bei den Monotrematen und den Marsupialiern. *Morph. Jb.* **28**: 147–178.
- Paulli, S. (1900b). Ueber die Pneumaticität des Schädels bei den Säugethieren. II. Ueber die Morphologie des Siebbeins und die Pneumaticität bei den Ungulaten und Probosciden. *Morph. Jb.* **28**: 179–251.
- Paulli, S. (1900c). Ueber die Pneumaticität des Schädels bei den Säugethieren. III. Ueber die Morphologie des Siebbeins und die Pneumaticität bei den Insectivoren Hyracoideen, Chiropteren, Carnivoren, Pinnipeden, Edentates, Rodentiern, Prosimien und Primaten. *Morph. Jb.* **28**: 483–564.
- Poran, N. S. (1998). Vomeronasal organ and its associated structures in the opossum *Monodelphis domestica*. *Microsc. Res. Tech.* **43**: 500–510.
- Proetz, A. W. (1953). *Essays on the Applied Physiology of the Nose*, 2nd Ed., Annals Publishing Company, St Louis, Missouri.
- Ressler, K. J., Sullivan, S. L., and Buck, L. B. (1993). A zonal organization of odorant receptor gene expression in the olfactory epithelium. *Cell* **73**: 597–609.
- Ressler, K. J., Sullivan, S. L., and Buck, L. B. (1994). Information coding in the olfactory system: Evidence for a stereotyped and highly organized epitope map in the olfactory bulb. *Cell* **79**: 1245–1255.
- Ridgway, S. H., Demski, L. S., Bullock, T. H., and Schwanzel-Fukuda, M. (1987). The terminal nerve in odontocete cetaceans. *Ann. N. Y. Acad. Sci.* **519**: 184–200.

- Rouquier, S., Blancher, A., and Giorgi, D. (2000). The olfactory receptor gene repertoire in primates and mouse: Evidence for reduction of the functional fraction in primates. *Proc. Natl. Acad. Sci. U.S.A.* **97**: 2870–2874.
- Rowe, T. (1986). Homology and evolution of the deep dorsal thigh musculature in birds and other Reptilia. *J. Morphol.* **198**: 327–346.
- Rowe, T. (1988). Definition, diagnosis and origin of Mammalia. *J. Vertebr. Paleontol.* **8**: 241–264.
- Rowe, T. (1993). Phylogenetic systematics and the early history of mammals. In: *Mammal Phylogeny: Mesozoic Differentiation, Multituberculates, Monotremes, Early Therians, and Marsupials*, F. S. Szalay, M. J. Novacek, and M. C. McKenna, eds., pp. 129–145, Springer-Verlag, New York.
- Rowe, T. (1996a). Coevolution of the mammalian middle ear and neocortex. *Science* **273**: 651–654.
- Rowe, T. (1996b). Brain heterochrony and evolution of the mammalian middle ear. In: *New Perspectives on the History of Life*, M. Ghiselin and G. Pinna, eds., pp. 71–96, California Academy of Sciences, Memoir 20.
- Rowe, T. (2004). Chordate phylogeny and development. In: *Assembling the Tree of Life*, M. J. Donoghue and J. Cracraft, eds., pp. 384–409, Oxford University Press, Oxford.
- Rowe, T., Carlson, W., and Bortorff, W. (1993). *Thrinaxodon: Digital Atlas of the Skull*, CD-ROM, First edition, for MS-DOS platform, 623 megabytes, University of Texas Press, Austin, Texas.
- Rowe, T., Carlson, W., and Bortorff, W. (1995). *Thrinaxodon: Digital Atlas of the Skull*, CD-ROM, 2nd Ed., for Windows and Macintosh platforms, 547 megabytes, University of Texas Press, Austin, Texas.
- Rowe, T., Kappelman, J., Carlson, W. D., Ketcham, R. A., and Denison, C. (1997). High-resolution computed tomography: A breakthrough technology for Earth scientists. *Geotimes* **42**: 23–27.
- Rowe, T., Brochu, C. A., Kishi, K., Colbert, M., and Merck, J. W. (1999). Introduction to *Alligator*: Digital atlas of the skull. In: *Cranial Morphology of Alligator and Phylogeny of Alligatoroidea*, T. Rowe, C. A. Brochu, and K. Kishi, eds., pp. 1–8, Society of Vertebrate Paleontology Memoir 6, *J. Vert. Paleontol.* **19**, Supplement to issue 2.
- Rubin, B. D., and Katz, L. C. (1999). Cortical imaging of odorant representations in the mammalian olfactory bulb. *Neuron* **23**: 499–511.
- Salazar, I., Quintiero, P. S., Cifuentes, J. M., Fernandez, P., and Lombardero, M. (1997). Distribution of the arterial supply to the vomeronasal organ in the cat. *Anat. Rec.* **247**: 129–136.
- Sánchez-Villagra, M. (2001). Ontogenetic and phylogenetic transformations of the vomeronasal complex and nasal floor elements in marsupial mammals. *Zool. J. Linn. Soc.* **131**: 459–479.
- Schmidt-Nielsen, K., Hainworth, F. R., and Murrish, D. F. (1970). Counter-current exchange in the respiratory passages: Effect on water and heat balance. *Respir. Physiol.* **9**: 263–276.
- Shapiro, L. S., Roland, R. M., and Haplern, M. (1997). Development of olfactory marker protein and N-CAM expression in chemosensory systems of the opossum *Monodelphis domestica*. *J. Morphol.* **234**: 109–129.
- Shipley, M. T., McLean, J. H., and Ennis, M. (1995). Olfactory System. In: *The Rat Nervous System*, 2nd Ed., G. Paxinos, ed., pp. 899–926, Academic Press, New York.
- Singer, A. G., Agosta, W. C., Clancy, A. N., and Macrides, F. (1987). The chemistry of vomeronasally detected pheromones: Characterization of an aphrodisiac protein. *Ann. N. Y. Acad. Sci.* **519**: 287–298.
- Stoddart, D. M. (ed.). (1980a). *Olfaction in Mammals*, Zoological Society of London, Symposium 45. Academic Press, London.
- Stoddart, D. M. (1980b). *The Ecology of Vertebrate Olfaction*. Chapman and Hall, London.
- Toeplitz, C. (1920). Bau und entwicklung des Knorpelschädels von *Didelphys marsupialis*. *Zoologica* **27**: 1–84.
- Touhara, K., Sengoku, S., Inaki, K., Tsuboi, A., Hirono, J., Sato, T., Sakano, H., and Haga, T. (1999). Functional identification and reconstitution of an odorant receptor in single olfactory neurons. *Proc. Natl. Acad. Sci. U.S.A.* **96**: 4040–4045.
- VandeBerg, J. L. (1990). The gray short-tailed opossum (*Monodelphis domestica*) as a model didelphid species for genetic research. *Austral. J. Zool.* **37**: 235–247.
- Van Valkenburgh, B., Theodor, J., Friscia, A., Pollack, A., and Rowe, T. (2004). Respiratory turbinates of canids and felids: A quantitative comparison. *J. Zool. Lond.* **264**: 1–13.
- Voss, R. S., and Jansa, S. A. (2003). Phylogenetic studies on didelphid marsupials II. Nonmolecular data and new IRBP sequences: Separate and combined analyses of didelphine relationships with denser taxon sampling. *Bull. Am. Mus. Nat. Hist.* **276**: 1–82.
- Watson, L. (1999). *Jacobson's Organ*, Penguin Press, London.
- Wible, J. R. (1991). Origin of Mammalia: The craniodental evidence reexamined. *J. Vertebr. Paleontol.* **11**: 1–28.
- Wible, J. R. (2003). On the cranial osteology of the short tailed opossum *Monodelphis brevicaudata* (Didelphidae, Marsupialia). *Ann. Carneg. Mus.* **72**: 137–202.
- Wirsig, C. R., and Leonard, C. M. (1987). Terminal nerve damage impairs the mating-behavior of the male hamster. *Brain Res.* **417**: 293–303.
- Witmer, L. M. (1995). Homology of facial structures in extant archosaurs (birds and crocodylians), with special reference to paranasal pneumaticity and nasal conchae. *J. Morphol.* **225**: 269–327.